1 **Evaluating soil moisture retrievals from ESA's SMOS and NASA's SMAP**

2 **brightness temperature datasets**

3

4 A. Al-Yaari (1); J.-P. Wigneron (1); Y. Kerr (2); N. Rodriguez-Fernandez (2); P. E. O'Neill

5 (3); T. J. Jackson (4); G.J.M. De Lannoy (5); A. Al Bitar (2); A. Mialon (2); P. Richaume (2);

6 J. P. Walker (6); A. Mahmoodi (2); and S. Yueh (7)

7 (1) INRA, UMR1391 ISPA, Villenave d'Ornon, France, amen.alyaari@bordeaux.inra.fr,

8 tel: 33 5 57 12 24 27, Fax: 33 5 57 12 24 20

9 (2) CESBIO, CNES/CNRS/IRD/UPS, UMR 5126, Toulouse, France

10 (3) NASA, Goddard Space Flight Center, Greenbelt, MD 20771, USA

11 (4) USDA-ARS Hydrology and Remote Sensing Laboratory, Beltsville, MD 20705-2350

12 USA

13 (5) KU Leuven, Department of Earth and Environmental Sciences, Heverlee, Belgium

14 (6) Department of Civil Engineering, Monash University, Clayton, Melbourne, Victoria,

15 Australia

16 (7) Jet Propulsion Lab., California Inst. of Technol., Pasadena, CA, USA

17

18

19 Keywords: SMOS, SMAP, soil moisture, statistical regression

20

21

22

Abstract

Two satellites are currently monitoring surface soil moisture (SM) using L-band observations: SMOS (Soil Moisture and Ocean Salinity), a joint ESA (European Space Agency), CNES (Centre national d'études spatiales), and CDTI (the Spanish government agency with responsibility for space) satellite launched on November 2, 2009 and SMAP (Soil Moisture Active Passive), a National Aeronautics and Space Administration (NASA) satellite successfully launched in January 2015. In this study, we used a multilinear regression approach to retrieve SM from SMAP data to create a global dataset of SM, which is consistent with SM data retrieved from SMOS. This was achieved by calibrating coefficients of the regression model using the CATDS (Centre Aval de Traitement des Données) SMOS Level 3 SM and the horizontally and vertically polarized brightness temperatures (TB) at 40° incidence angle, over the 2013 - 2014 period. Next, this model was applied to SMAP L3 TB data from Apr 2015 to Jul 2016. The retrieved SM from SMAP (referred to here as SMAP_Reg) was compared to: (i) the operational SMAP L3 SM (SMAP_SCA), retrieved using the baseline Single Channel retrieval Algorithm (SCA); and (ii) the operational SMOSL3 SM, derived from the multiangular inversion of the L-MEB model (L-MEB algorithm) (SMOSL3). This inter-comparison was made against *in situ* soil moisture measurements from more than 400 sites spread over the globe, which are used here as a reference soil moisture dataset. The *in situ* observations were obtained from the International Soil Moisture Network (ISMN; https://ismn.geo.tuwien.ac.at/) in North of America (PBO_H2O, SCAN, SNOTEL, iRON, and USCRN), in Australia (Oznet), Africa (DAHRA), and in Europe (REMEDHUS, SMOSMANIA, FMI, and RSMN). The agreement was analyzed in terms of four classical statistical criteria: Root Mean Squared Error (RMSE), Bias, Unbiased RMSE (UnbRMSE), and correlation coefficient (R). Results of the comparison of these various products with *in situ* observations show that the performance of

48 both SMAP products i.e. SMAP_SCA and SMAP_Reg is similar and marginally better to

49 that of the SMOSL3 product particularly over the PBO_H2O, SCAN, and USCRN sites.

50 However, SMOSL3 SM was closer to the *in situ* observations over the DAHRA and Oznet

51 sites. We found that the correlation between all three datasets and *in situ* measurements is

52 best (R > 0.80) over the Oznet sites and worst (R = 0.58) over the SNOTEL sites for

53 SMAP_SCA and over the DAHRA and SMOSMANIA sites (R= 0.51 and R= 0.45 for

54 SMAP_Reg and SMOSL3, respectively). The Bias values showed that all products are

55 generally dry, except over RSMN, DAHRA, and Oznet (and FMI for SMAP_SCA). Finally,

56 our analysis provided interesting insights that can be useful to improve the consistency

57 between SMAP and SMOS datasets.

58

59

60

61

62

63

64

65

66

67

68

69

70

71

72

1. Introduction

Lately, the importance of soil moisture has become increasingly apparent, because soil moisture is a key variable in better understanding of the land-atmosphere interactions (Chen et al., 2016; Hirschi et al., 2014). The exchange of heat and water between the land surface and atmosphere is influenced by soil moisture (Berg et al., 2014; Hupet & Vanclooster, 2002; Seneviratne et al., 2010; Western et al., 2004), which was recognized as an Essential Climate Variables (ECV) in 2010 (GCOS, 2010).

Global soil moisture information has become available via different active and passive microwave remote sensing techniques with good temporal and spatial resolutions (Bartalis et al., 2007; Kerr et al., 2001; Njoku et al., 2002; Njoku et al., 2003; Owe et al., 2001; Ulaby et al., 1996; Wigneron et al., 1995). However, the required temporal and spatial resolutions strongly depend on the applications (e.g., agricultural applications vs. climate studies). Recently, new global soil moisture datasets, with a typical target accuracy of 0.04 m^3/m^3 (Jackson et al., 2016; Kerr et al., 2010; Kerr et al., 2012) over bare, low vegetation cover, and sparsely vegetated areas, have been produced based on microwave satellite observations at L-band (1.4 GHz, 21 cm). L-band is considered optimal for soil moisture monitoring (Kerr et al., 2001; Njoku et al., 2003; Wang & Choudhury, 1981) due to its higher sensitivity to soil moisture and penetration into vegetation and soil (Kerr, 2007; Njoku et al., 2003; Owe & Van de Griend, 1998; Wang & Choudhury, 1981) than other higher frequencies (e.g., C-band, X-band, etc.). The new L-band based datasets include surface soil moisture from two spaceborne missions: ESA's (European Space Agency) Soil Moisture and Ocean Salinity (SMOS) (Kerr et al., 2012) and NASA's (National Aeronautics and Space Administration) Soil Moisture Active Passive (SMAP) (Entekhabi et al., 2010). The SMOS and SMAP satellites were launched in 2009 and 2015, respectively, and have been providing microwave brightness temperature (TB) observations since then. Soil moisture information is retrieved

from SMAP's and SMOS's TB observations based on the principle that soil TB is mainly determined by soil moisture via soil dielectric constant (Njoku et al., 2002; Schmugge et al., 1976; Ulaby et al., 1996). Nevertheless, the sensitivity of the SMOS and SMAP TB observations to soil moisture is reduced by perturbing factors such as vegetation (attenuation of the emission from the soil and additional upwelling emission toward the space-borne sensor), surface roughness (scattering effects increase the emitting surface area), topography, soil texture, soil bulk density, and soil temperature (Choudhury et al., 1979; Grant et al., 2008; Holmes et al., 2006; Jackson & Schmugge, 1991; Kerr et al., 2012; Njoku & Li, 1999; Njoku et al., 2003; Wang et al., 1983; Wigneron et al., 2007; Wigneron et al., 2011).

There are several remotely sensed soil moisture products available (in addition to SMOS and SMAP); however, these cover different periods and are not consistent in terms of spatial and temporal resolutions, period availability, grid, etc. Given the wide availability of soil moisture datasets retrieved from different microwave observations, studies focusing on the merging of these products are important to advance in the field of producing long-term and consistent datasets of several climatic variables. A great effort has been made by the scientific community in the last decade to build a coherent and consistent long term soil moisture datasets such as the ESA Climate Change Initiative (CCI) soil moisture data record (e.g., Enenkel et al., 2015; Liu et al., 2012; http://www.esa-soilmoisture-cci.org/; Wagner et al., 2012), deemed necessary for global soil moisture monitoring, drought monitoring, climate forecasts, etc. The CCI product is estimated based on a posteriori merging i.e. merging the retrieved soil moisture datasets based on the relative errors of soil moisture products and a CDF (cumulative distribution function)-matching used to rescale the different soil moisture products into a common climatology. An alternative approach is to use data fusion i.e. merging of microwave datasets prior to the retrieval (e.g., through the use of a common retrieval algorithm as proposed later in this paper). This method allows better exploitation of

the complimentary of information provided by the different sensors not included in the posteriori combination approach (Aires et al., 2012; Kolassa et al., 2013). A recent project was established by ESA to investigate the integration of SMOS soil moisture estimates within the CCI soil moisture data record using three approaches that implement the data fusion strategy:

(i)   multi-linear regression (Al-Yaari et al., 2016);

(i)   neural networks (Rodríguez-Fernández et al., 2015); and

(ii)   the Land Parameter Retrieval Model (LPRM; Van der Schalie et al., 2016).

Al-Yaari et al. (2016), for instance, demonstrated the efficiency of physically-based multiple-linear regression equations (Wigneron et al., 2004), referred to here as Linear Regression Method (LRM) in the following, to retrieve soil moisture from the Advanced Microwave Scanning Radiometer Earth Observing System (AMSR-E) TB observations. The LRM has several advantages: quickness, simplicity, and no strong demand on auxiliary datasets (Al-Yaari et al., 2016) such as the normalized difference vegetation index (NDVI) product used by the SMAP Single Channel Algorithm (SMAP_SCA), to estimate vegetation effects. The purpose of that initial study was to extend the SMOS soil moisture product into the past i.e., 2003-2009, using AMSR-E TB observations. The current study follows the same strategy to retrieve soil moisture from SMAP TB observations (SMAP_Reg) with a purpose to improve the temporal sampling rate together with the SMOS soil moisture product at the global scale. The main interest in the SMAP-Reg soil moisture product is that it is fully consistent with the SMOS Level 3 soil moisture product, as the regression equations are calibrated based on SMOS Level 3 data (soil moisture and TB). Furthermore, the idea here is to re-build a coherent and consistent soil moisture data set rather than to develop a new algorithm or to surpass the well-established radiative transfer models (e.g. the L-band Microwave Emission of the Biosphere (L-MEB) model, LRPM, etc.).

6

148   To this end, two specific objectives of this study are listed below:

149   (i)   produce a soil moisture product (SMAP_Reg) from SMAP TB that is consistent

150   with SMOS soil moisture retrievals using physically-based regression equations; and

151   (ii) compare SMAP_Reg with operational SMAP and SMOS soil moisture retrievals

152   against ground-based soil moisture measurements.

153   Since SMAP soil moisture products are relatively recent, their evaluation and their

154   inter-comparison with other soil moisture data sets are required (Chan et al., 2016; Zeng et

155   al., 2016). To advance our goal, therefore, the second objective of this study is two-fold: to

156   evaluate the SMAP_Reg product, and to carry out a first evaluation of the agreement

157   between SMAP and SMOS level 3 soil moisture products on global scale and against

158   ground-based measurements (sparse and dense networks). The aim is not to establish which

159   product is more accurate with respect to *in situ* but to understand the spatio-temporal

160   patterns of SMAP relative to SMOS and how SMAP differs from SMOS globally. The

161   agreement and degree of dispersion between the SMAP and SMOS soil moisture products

162   are analyzed here in terms of four classical statistical criteria: Root Mean Squared Error

163   (RMSE), Bias, Unbiased RMSE (UnbRMSE), and correlation coefficient (R) during the

164   overlapping period (from Apr 2015 to Jul 2016).

165   The datasets, the local regression method, and the evaluation metrics used in this study

166   are described in Section 2. Results are presented in Section 3. Finally, discussion and

167   conclusions are provided in Section 4 and Section 5, respectively.

2. Materials and methods

2.1 Datasets

2.1.1 SMOS level 3 TB and soil moisture products

SMOS is a joint ESA, CNES (Centre national d'études spatiales), and CDTI (the Spanish government agency with responsibility for space) mission that was launched on November 2, 2009 (Kerr et al., 2012). The SMOS satellite carries an interferometric radiometer that operates at L-band, with multiple incidence angles, a spatial resolution of 35 km at the center of the field of view, a revisit time of 3 days, and ascending and descending overpass at 6:00 AM (local time) and 6:00 PM, respectively (Kerr et al., 2001; Kerr et al., 2010). Global SMOS Level 3 gridded multi-angular TB and soil moisture (top 0-5 cm surface layer) products (SMOSL3; version R04+OPER) are generated and provided by the CATDS (Centre Aval de Traitement des Données) center in France (Kerr et al., 2013). The SMOSL3 products are delivered for both orbits i.e. ascending and descending, projected on a global EASE (Equal Area Scalable Earth) grid (V2) 25 km, by the CATDS, and are available online via http://www.catds.fr/. The IFS (Integrated Forecast System) soil temperature product from the European Centre for Medium-Range Weather Forecasts (ECMWF) is used in the SMOSL3 algorithm to retrieve the SMOSL3 soil moisture.

SMOSL3 TB product provides multi-angular TB data (in Kelvin) at the top of the atmosphere, i.e. *not* at the surface level and without correction for select reflected extraterrestrial sky (e.g., cosmic and galactic) and atmosphere contributions, but after projection onto the Earth reference frame (unlike the operational Level 2 product). The multi-angular TB are binned and averaged in 5°-width incidence angle bins with the center ranging from 2.5° to 62.5°. CATDS has recently provided SMOSL3 TB at 40°, and for this purpose

191   the multi-angular TB are binned and averaged in 2º-width incidence angle bins. SMOSL3 soil

192   moisture products (provided in m^3/m^3) are derived from the multiangular inversion of the L-

193   MEB model (L-MEB algorithm) (Wigneron et al., 2007), i.e. the same method used for Level

194   2 soil moisture retrieval (Kerr et al., 2012), but are improved by using several revisits

195   simultaneously (Kerr et al., 2016). SMOS TBs for ascending passes only and their associated

196   soil moisture retrievals were used in this study (Al-Yaari et al., 2014a; Al-Yaari et al., 2014b)

197   for a better consistency with SMAP soil moisture retrieval datasets, which are only provided

198   at 6:00 AM.

199   Radio Frequency Interferences (RFI) originating from man-made emissions have been

200   shown to affect the quality of the SMOS TB observations (Oliva et al., 2012). RFI probability

201   is used to filter the SMOS datasets. This probability is the total number of deleted TBs due to

202   suspected RFI on a certain period divided by the total number of TB measurements acquired

203   during the same period available in the SMOS L1C datasets. In this study, SMOS TB and soil

204   moisture data were excluded when the RFI probability is higher than 20% following Kerr et

205   al. (2016). The reader is referred to the Algorithm Theoretical Based Document (Kerr et al.,

206   2013) for more details on the SMOSL3 products.

207   **2.1.2   SMAP level 3 TB and soil moisture products**

208   SMAP is a NASA satellite that was launched on January 31, 2015. The SMAP

209   satellite at launch carried two instruments: a Synthetic Aperture Radar and a radiometer

210   operating at L-band, with a fixed incidence angle of 40º, a spatial resolution of 40 km, a

211   revisit of 2-3 days and ascending and descending overpass at 6:00 PM (local time) and 6:00

212   AM, respectively (Entekhabi et al., 2010; Piepmeier et al., 2016). Soil moisture (top 0-5 cm

213   surface layer) and freeze/thaw were supposed to be provided with three spatial resolutions

214   ~3 km (high-resolution from radar), ~9 km (intermediate-resolution from radar and

215   radiometer), and ~36 km (low-resolution from radiometer), projected on the EASE V2 grid.

216   However, the radar instrument onboard SMAP satellite stopped transmitting data on Jul 7,

217   2015 due to a problem in the radar's high-power amplifier (Chan et al., 2016). Currently, soil

218   moisture products are retrieved from SMAP TB radiometer data using the baseline Single

219   Channel Algorithm (SCA) V-pol (Chan et al., 2016; Jackson, 1993). The global daily SMAP

220   level 3 V3 gridded descending brightness temperature (at both H and V polarizations) and

221   soil moisture (which is a compilation of 24 hrs of L2 soil moisture orbits) products,

222   henceforth referred to here as SMAP_SCA, on EASE 2 grid (36 km) were used in this study.

223   Unlike the SMOSL3 TBs product, the TBs provided within the SMAP L3 product are

224   calibrated at the surface level, i.e. corrected for Sky radiation and atmosphere contributions

225   using auxiliary near surface information (De Lannoy et al., 2015). The SMAP L2 half-orbit

226   soil moisture product (and also the SMAP L3 soil product) uses ancillary data (including soil

227   temperature information) from the NASA's Global Modeling and Assimilation Office

228   (GMAO/GEOS-5) Forward Processing product, which is provided with SMAP datasets. They

229   are freely available from the National Snow and Ice Data Center (NSIDC). For more details

230   on the SMAP mission and SMAP passive products, the reader is referred to (Chan et al.,

231   2016; Piepmeier et al., 2016) and the SMAP Level 2 & 3 Soil Moisture (Passive) Algorithm

232   Theoretical Basis Document (SMAP_ATBD) available here:

233   https://nsidc.org/data/docs/daac/smap/sp_l2_smp/pdfs/L2_SM_P_ATBD_v7_Sep2015-po-

234   en.pdf.

235   Furthermore, it should be noted that both the SMOS and SMAP TB and soil moisture

236   datasets were filtered prior to the regression analysis and the evaluations. A pixel was masked

237   out when:

238   (i) it is not considered as "Land" in the United States Geological Survey (USGS)

239   Land-Sea mask (water fraction above 10%)";

240   (ii) it is classified as "Urban and Built-Up", "Snow and Ice", "Water", "Permanent

241   Wetlands", "Evergreen Needleleaf Forest", or "Evergreen Broadleaf Forest"

242   according to the International Geosphere Biosphere Programme (IGBP) land

243   cover map;

244   (iii) the number of retrievals < 15 over the whole retrieval period;

245   (iv) it corresponds to a date where the MERRA-Land soil temperature is < 274 K (to

246   avoid frost and frozen conditions);

247   (v) SMOS TB is estimated to be not sensitive to the surface effects according to the

248   mask developed by Parrens et al. (2016); and

249   (vi) it corresponds to a date that is not recommended for retrieval based on the SMAP

250   quality flag.

251   **2.1.3 MERRA-Land soil temperature**

252   The soil temperature product was extracted from the NASA MERRA-Land product,

253   which is a land-surface model forced with atmospheric reanalysis fields (precipitation

254   corrected using gauges) (Reichle et al., 2011). MERRA_Land is a supplemental land surface

255   data product of the Modern-Era Retrospective analysis for Research and Applications

256   (MERRA) datasets, produced by the Goddard Earth Observing System model and

257   assimilation system. MERRA-Land uses an updated catchment land surface model (version

258   Fortuna-2.5) and includes a gauge-based precipitation data from the NOAA Climate

259   Prediction Centre. The accuracy and precision of MERRA-Land soil temperature were

260   assessed and analyzed by Parinussa et al. (2011) and Holmes et al. (2012). These studies

261   found the performance of MERRA-Land to be similar to the ECMWF soil temperature

262   products. The MERRA-Land product is available for the 1980-February 2016 period,

263   provided with high temporal resolution (hourly) and a horizontal resolution of 2/3° longitude

264   by 1/2° latitude (http://gmao.gsfc.nasa.gov/research/merra/merra-land.php). The follow-up

265   re-analysis product is MERRA2. It has improved soil temperature estimates, and uses gage

266   information to correct the precipitation (Reichle et al., 2016), similarly to (but not exactly the

267   same as) MERRA-Land. At the time of writing, the MERRA2 product was not yet available.

268   Consequently, this study uses MERRA-Land auxiliary information.

269   **2.1.4 ECMWF soil temperature**

270   The global atmospheric reanalysis ERA-Interim soil temperature datasets obtained from

271   ECMWF were used in this study. The Hydrology-Tiled ECMWF Scheme for Surface

272   Exchange over Land (H-TESSEL) is used by the ECMWF forecasts to solve for several

273   parameters including a four-layer soil temperature profile (Balsamo et al., 2009). In this

274   study, the soil temperature from the first layer (0–0.07 m) provided at 00:00, 06:00, 12:00,

275   18:00 UTC over a grid with a space sampling of 0.25×0.25 degrees was used. The ECMWF

276   product is available from 1979 to present. The ECMWF datasets can be freely accessed at:

277   http://apps.ecmwf.int/datasets/ and more information can be found in Berrisford et al. (2011).

278   **2.1.5 Ground-based measurements**

279   Validation of remotely sensed soil moisture products against ground-based

280   measurements is a necessary step before any use. Nowadays several soil moisture networks

281   share ground-based soil moisture measurements via the website of the International Soil

282   Moisture Network (ISMN; Dorigo et al., 2011; Dorigo et al., 2015). ISMN is an ESA funded

283   project initiated through the SMOS CAL/VAL. Data can be freely obtained from ISMN at

284   https://ismn.geo.tuwien.ac.at/. All sites from ISMN that provide soil moisture within the

285   period of Apr 2015- Jul 2016 were used in this study to evaluate the remotely sensed soil

286   moisture products. Most of the sites are located in different regions with different vegetation,

287   climate, and soil conditions.

288   Eleven networks in North America, Australia, Africa, and Europe were used namely:

289   the PBO_H2O (http://xenon.colorado.edu/portal) network (Larson et al., 2008), the SCAN

290   (Soil Climate Analysis Network) network (http://www.wcc.nrcs.usda.gov/scan/) (Schaefer et

291   al., 2007), the SNOTEL (Snow Telemetry) network (http://www.wcc.nrcs.usda.gov/snow/),

292   the USCRN (U.S. climate reference) network (Bell et al., 2013), the newly built RSMN

293   (Romanian Soil Moisture & Temperature Observation Network) network

294   (http://assimo.meteoromania.ro/) in Romania, the FMI (Finnish Meteorological Institute)

295   network (Rautiainen et al., 2012) in Finland, the Oznet (Australian Moisture Monitoring

296   Network) network (Smith et al., 2012) in Australia, the SMOSMANIA (Soil Moisture

297   Observing System–Meteorological Automatic Network Integrated Application) network

298   (Albergel et al., 2008; Calvet et al., 2007) in France, the DAHRA network (Tagesson et al.,

299   2015) in Senegal, the iRON (Integrated Roaring Fork Observation Network) network

300   http://ironagci.blogspot.co.at/, and the REMEDHUS (Soil Moisture Measurement Stations

301   network of the University of Salamanca) network (Sanchez et al., 2012) in Spain. To ensure

302   the high quality of the *in situ* measurements and to minimize the systematic differences

303   between them and the remotely-sensed soil moisture products, we restricted the validation

304   step to sites with a top soil layer of ~ 0 - 5 cm and with a minimum number of temporal 15

305   measurements. ISMN quality flags associated with the soil moisture data were applied

306   (Dorigo et al., 2013). Consequently, ~ 400 (out of ~ 1000) sites from 11 networks were used

307   for the evaluation. Moreover, if multiple sensors fall within one pixel, each sensor is treated

308   independently: in this paper, unlike (De Lannoy & Reichle, 2015) we will not seek to

309   construct reliable statistical confidence intervals. Fig. 1 shows the locations of the different *in*
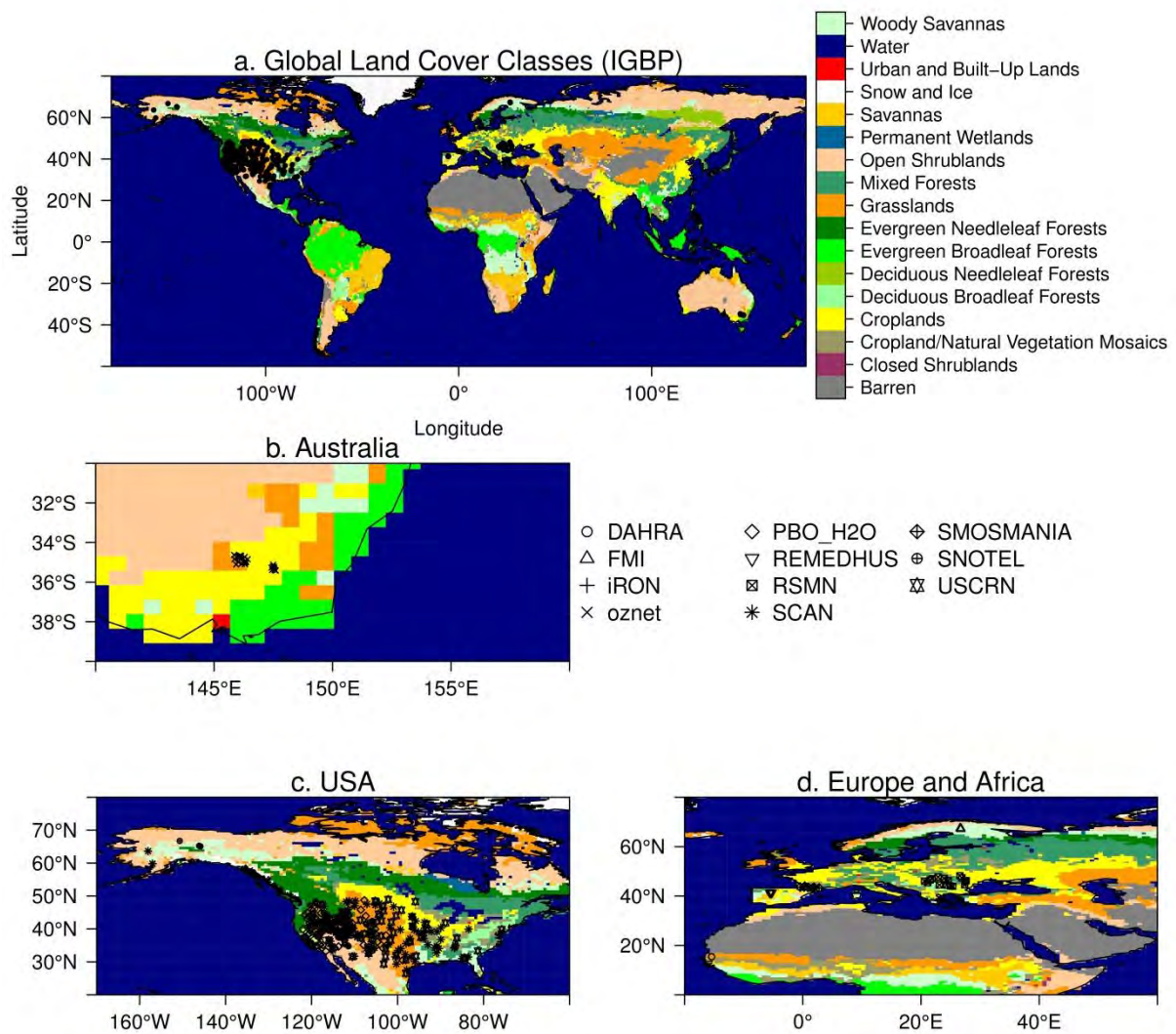
310   *situ* soil moisture sites.

311

Fig. 1 IGBP (International Geosphere Biosphere Programme) land cover classification (Friedl et al., 2010) with the locations of the different *in situ* soil moisture sites (a) over Australia (b), the USA (c), and Africa and Europe (d).

2.2 Methodology

The methodology used in this study to retrieve soil moisture from SMAP TB based on regression coefficients, obtained from SMOS TB and soil moisture, is schematized in Fig. 2. It consists of two steps: the calibration and the data production.
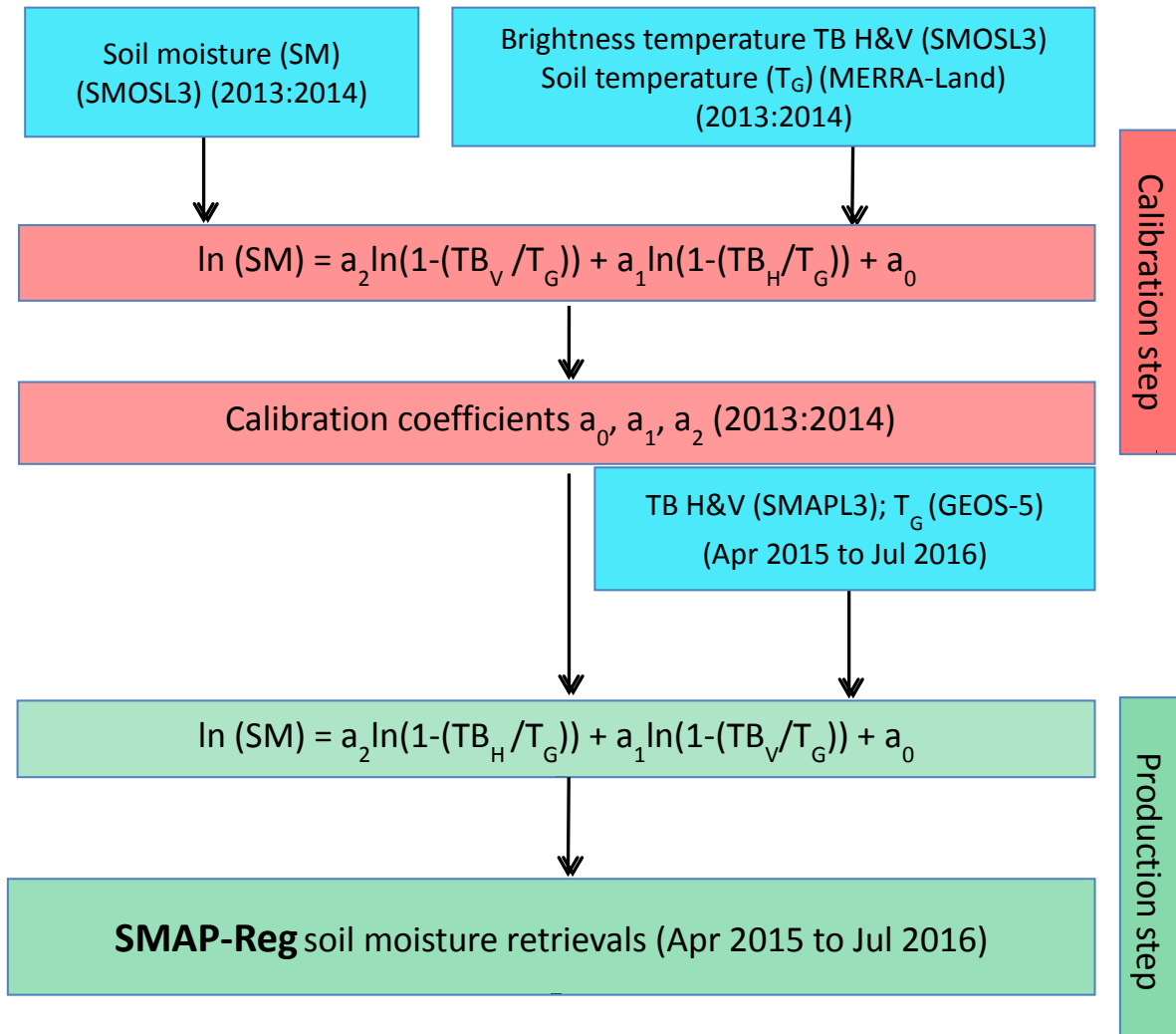
Fig. 2 The LRM (local regression method) algorithm: inputs (in blue), calibration step (in red), and soil moisture production step (in green).

2.2.1 Calibration

A regression equation was analytically derived from the general (tau-omega) model equations (Mo et al., 1982) by Wigneron et al. (2004):

$$\ln(SM) = a_0 + a_1 \ln(\Gamma_H) + a_2 \ln(\Gamma_V) \tag{1}$$

332   Where a_0, a_1, and a_2 are regression coefficients, and the first (second) term on the right hand

333   side of Eq. (1) represents the surface reflectivity at horizontal (vertical) polarization (Γ_P),

334   described as:

335   $\Gamma_P = 1 - \dfrac{T_{BP}}{T_G}$ (2)

336   where:

337   T_{BP} is the brightness temperature at polarization p (H or V) at 40° incidence angle and T_G is

338   the surface soil temperature.

339   We used a multiple linear regression i.e., a statistical technique that predicts the

340   outcome of a response (dependent) variable using two or more independent (explanatory)

341   variables. The coefficients of Eq. (1) were estimated using ordinary least squares techniques

342   that minimize the sum of the squared errors. Eq. (1) was used in this study to retrieve soil

343   moisture from the SMAP L-band TB observations. The coefficients a_0, a_1, and a_2 of Eq. (1)

344   were calibrated per land cover category (obtained from the IGBP land cover map (see Fig. 1))

345   using the most recent available re-processed SMOS datasets: the SMOS TB in both V and H

346   polarizations at incidence angle of 40° and soil moisture, and MERRA T_G datasets. The

347   calibration was done during the 2013-2014 period. Note that this calibration was made here

348   per land cover category, and not on a pixel to pixel basis as it was made previously in most

349   LRM studies based on space-borne observations (Al-Yaari et al., 2016; Parrens et al., 2012;

350   Saleh et al., 2006). This choice was made here to increase the spatial coverage. SMOS TBs

351   observations are highly affected by RFI and therefore most of the regions in Europe and Asia

352   would be masked out. To overcome this issue, we removed pixels with high RFIs and then we

353   calibrated the regression equation with the rest of pixels within each land cover category.

354   Lastly, we applied the obtained coefficients to the SMAP TB data (which are less impacted by

355   RFI) for all the pixels for each land cover category.

2.2.2 Soil moisture production

Soil moisture was computed from the SMAP TB data for the Apr 2015 - Jul 2016 period using the regression coefficients computed in the calibration step using Eq. (1). This was done given the fact that we have all inputs for Eq. (1) to compute the soil moisture: TB observations at both polarizations from SMAP, T_G datasets based on the GMAO GEOS-5 (here in after referred to as GEOS-5) model provided with the SMAP datasets (or any other source like ECMWF), and the coefficients (a_0, a_1, and a_2) from the calibration step.

2.3 Metrics used for evaluating the soil moisture data set

The SMAP_Reg soil moisture product, obtained using the LRM algorithm, was compared with the SMAP and SMOS official Level 3 soil moisture products, and all three remotely sensed soil moisture products were evaluated against *in situ* observations. This was achieved using classical metrics: Root Mean Square Error (RMSE; m^3/m^3), Bias (m^3/m^3), UnbRMSE (m^3/m^3) (Entekhabi et al., 2010), and the (Pearson) correlation coefficient (R), which can be computed as follows:

$$Bias = \frac{1}{N} \sum_{i=1}^{N} S_i - O_i \tag{3}$$

$$RMSE = \sqrt{\frac{1}{N} \sum_{i=1}^{N} (S_i - O_i)^2} \tag{4}$$

$$UnbRMSE = \sqrt{RMSE^2 - bias^2} \tag{5}$$

17

$$R = \frac{1}{(N-1)} \sum_{i=1}^{N} \left(\frac{S_i - \bar{S}}{\sigma_S} \right) \left(\frac{O_i - \bar{O}}{\sigma_O} \right) \qquad (6)$$

375   where the overbar indicates the mean;

376   • S_i is the ith remotely sensed soil moisture value;

377   • O_i is the ith *in situ* observed or the remotely sensed soil moisture value;

378   • N is the total number of observations; and

379   • σ_o and σ_s are the standard deviations of the *in situ* observed or remotely sensed soil

380   moisture values, respectively.

381   Moreover, Taylor diagrams (Taylor, 2001) were used in this study to compare in a

382   comprehensive way the remotely sensed soil moisture and the *in situ* soil moisture

383   measurements. Three statistics are summarized in a Taylor Diagram: the normalized standard

384   deviation (SDV) displayed as a radial distance, the correlation coefficient (R) displayed as an

385   angle in the polar plot, and the centered RMSE (displayed as the distance to the point

386   (observed) where R and SDV are equal to one). The performance of the remotely sensed soil

387   moisture products is considered closest to ground measurements with the shortest distance to

388   R = 1 and SDV = 1.

389

390

391

392

3   Results

3.1   SMAP and SMOS inter-comparison

Before presenting the regression analyses and evaluating the SMAP_Reg soil moisture product, it is necessary to evaluate and compare the measured (retrieved) Tb's (soil moisture) from SMOS and SMAP, which is the key to understand the different results, as it is the only input that changes between the SMAP and SMOS-based SM retrieval algorithms. For instance, this could help explain the differences in Bias, RMSE and correlation obtained between the different soil moisture products evaluated in this study over the different networks. For this purpose, global maps of R, RMSE, Bias, and UnbRMSE between SMAP and SMOS TBs and soil moisture were produced. Fig. 3 shows the global maps between SMOS and SMAP TBs during the Apr 2015 Jul 2016 period at both polarizations vertical (V-pol; left) and horizontal (H-pol; right): (a& e) correlation, (b& f) RMSE, (c& g) Bias, and (d &h) UnbRMSE. In general, there is a good agreement between SMOS and SMAP TBs at both V-pol and H-pol particularly in terms of temporal dynamics (R mostly > 0.8). The RMSE and UnbRMSE values are lower between SMAP and SMOS at V-pol than between SMAP and SMOS at H-pol over some regions (e.g., region of western North Africa). The RMSE (UnbRMSE) values range mostly between 2 and 8 (4) K over most of the globe except over some regions (e.g., Western Europe). SMAP presents cold (warm) bias with respect to SMOS over most of the globe (high latitude regions).

412

413
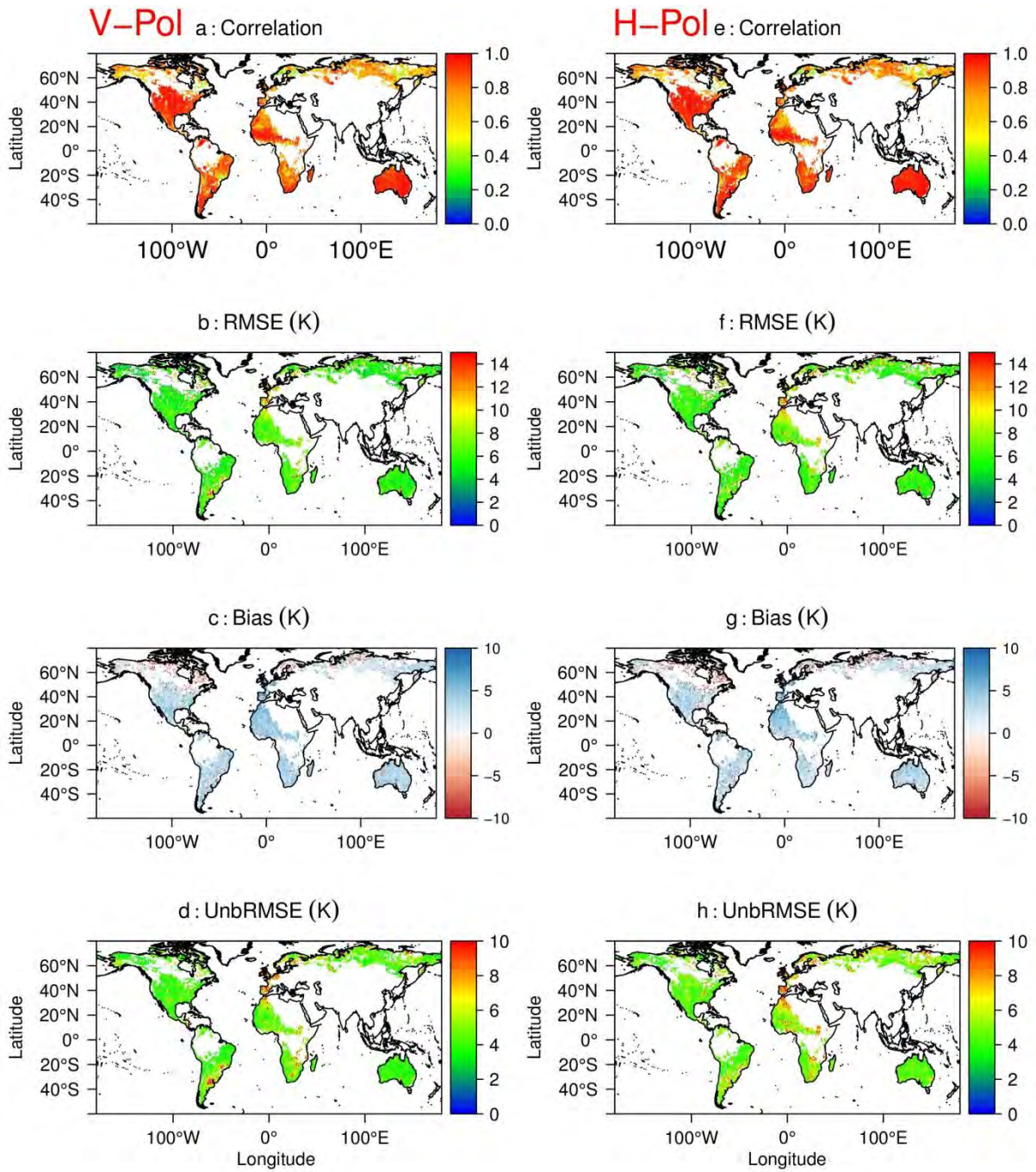
Fig. 3 Global inter-comparison between SMOS and SMAP TBs during the Apr 2015-Jul 2016 at both polarizations vertical (V-pol; left) and horizontal (H-pol; right): (a & e) correlation, (b & f) RMSE, (c & g) Bias, and (d &h) UnbRMSE. Pixels with a number of observations lower than 15 are indicated as blank areas.

418

419

420   Fig. 4 displays global inter-comparison between the operational SMOS (L3) and

421   SMAP (SCA) soil moisture retrievals during the Apr 2015- Jul 2016 period: (a) correlation,

422   (b) RMSE, (c) Bias, and (d) UnbRMSE. The correlations between SMOS and SMAP soil

423   moisture retrievals (Fig. 4a) are very high (between 0.8 and 1) over Australia, central Asia

424   and USA, and the Sahel, while moderate and low correlations are found over the other

425   regions. SMAP is much wetter under regions where the vegetation is moderate or high as

426   well as on coastlines, whereas SMOS is wetter over India and Central America, and far north

427   (see Fig. 4c). It can be seen in Figs. 4(b& d) that higher values of RMSE and UnbRMSE are

428   found in regions where the vegetation is moderate or high than over arid and semi-arid

429   regions. The retrieved soil moisture data from both SMOS and SMAP seem to agree

430   generally well in terms of unbRMSE (mostly < 0.05 m^3/m^3).

431
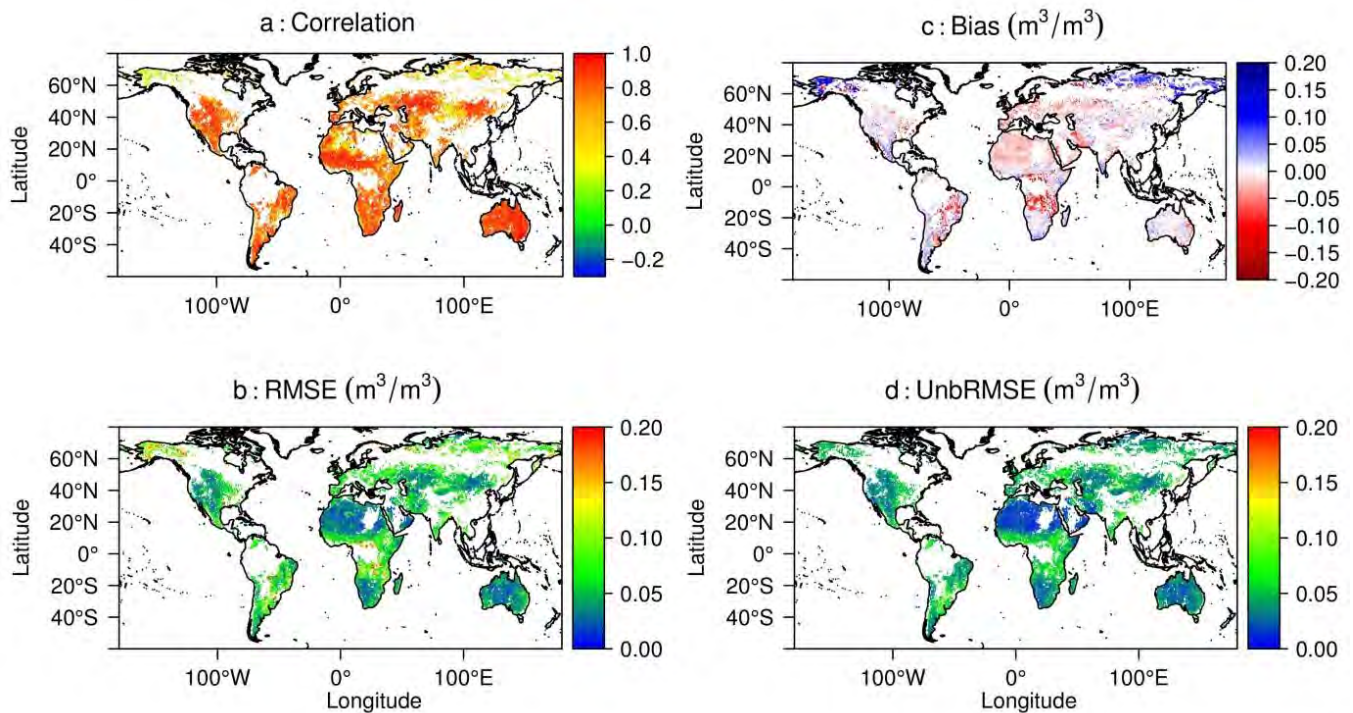
Fig. 4 Global inter-comparison between SMOS and SMAP soil moisture retrievals during the
Apr 2015-Jul 2016: (a) correlation, (b) RMSE, (c) Bias, and (d) UnbRMSE. Pixels with a
number of observations lower than 15 are indicated as blank areas.

3.2   Regression calibration

The regression coefficients a_0 (intercept coefficient), a_1 (coefficient for the H polarized TB), and a_2 (coefficient for the V polarized TB) in Eq. (1), obtained using SMOSL3 TB (V & H) and soil moisture in the calibration step, are presented in Table 1 and Fig. 5. A unique coefficient value for each land cover category was obtained. It can be seen that the values of the coefficient for the different land cover categories can be clearly distinguished. For instance, lowest coefficients values for a_0 and a_2 were obtained over "Closed shrublands"and highest over "Deciduous needleleaf forest" for a_2 and "Deciduous broadleaf forest" for a_0 while lowest values for a_1 were obtained over "Cropland/Natural vegetation mosaic" and highest over "Deciduous broadleaf forest".

Table 1 Regression coefficients of Eq. 1 calibrated using SMOS Level 3 TB and soil moisture in 2013-2014: a_0 represents the intercept, a_1 and a_2 represent the slope of regression line corresponding to H-pol and V- pol, respectively.

Land cover class	a_0	a_1	a_2
Deciduous Needleleaf forest	2.671	1.322	0.937
Deciduous Broadleaf forest	5.184	2.713	0.889
Mixed forest	3.848	2.485	0.492
Closed shrublands	0.789	1.068	0.242
Open shrublands	0.952	0.864	0.478
Woody savannas	3.212	1.903	0.643
Savannas	1.821	1.534	0.336
Grasslands	0.937	1.032	0.391
Croplands	0.815	0.867	0.421
Cropland/Natural vegetation mosaic	0.874	0.626	0.558
Barren or sparsely vegetated	1.049	1.830	0.384

450

451
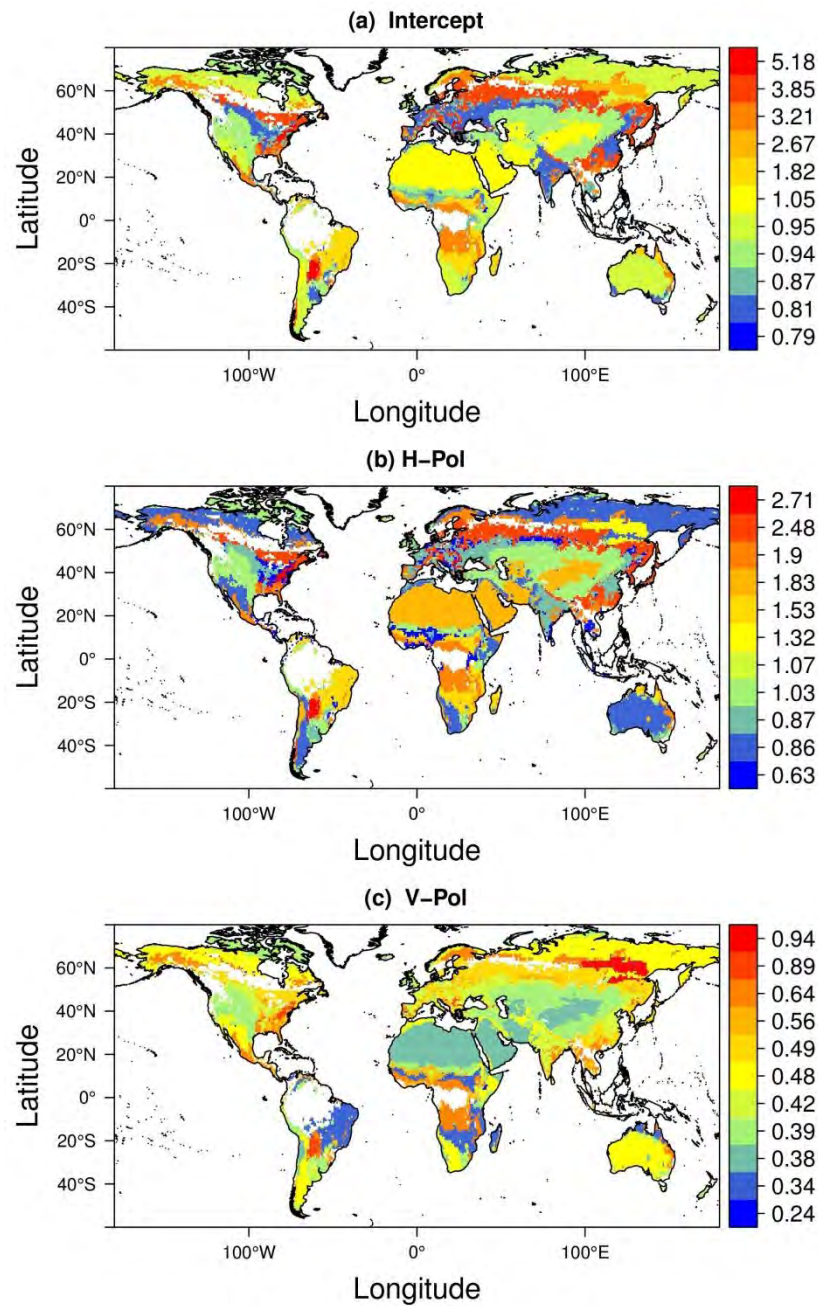
Fig. 5 Regression coefficients of Eq. 1 calibrated using SMOS Level 3 TB and soil moisture in 2013-2014 (a): intercept (a_0), (b) slope of regression line corresponding to the horizontal polarization (a_1), and (c) slope of regression line corresponding to the vertical polarization (a_2).

In order to make a first evaluation of the quality of the calibration step, and before applying the LRM algorithm to the SMAP TB data, we applied the LRM equations to the SMOS TB data. The soil moisture product (SMOS_Reg) was retrieved from SMOSL3 TB

459   using the regression coefficients computed from Eq. (1) over the calibration period. Then,

460   SMOS_Reg was compared with the reference SMOSL3 soil moisture for the same period in

461   terms of RMSE and correlation coefficient (P-value < 0.05).

462
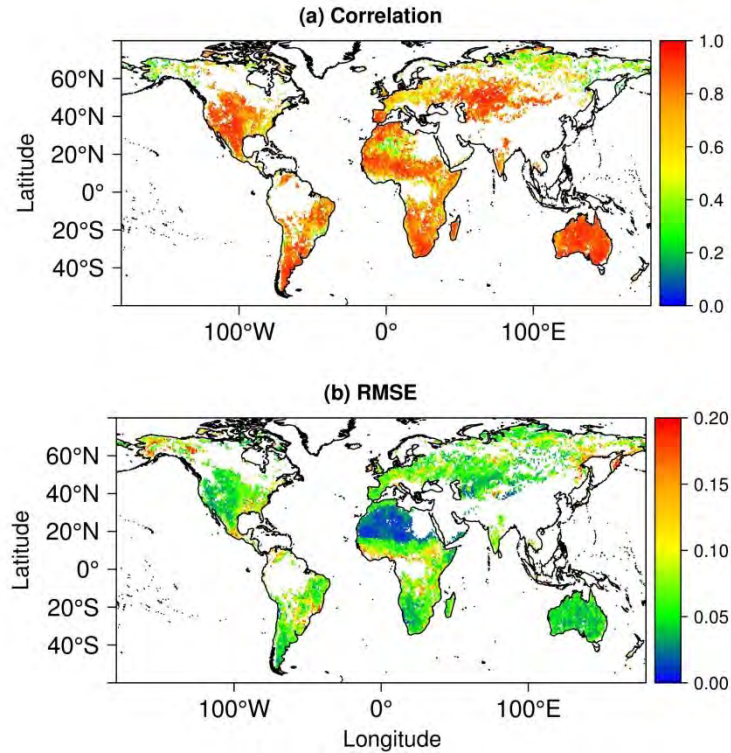
463   **Fig. 6** Comparison between the soil moisture values computed from the SMOS TB data using
464   LRM (SMOS_Reg) and the SMOS official level 3 soil moisture product in 2013-2014: (a)
465   correlation, R and (b) RMSE (m^3/m^3). Pixels with a number of observations lower than 15 are
466   indicated as blank areas.

467

468   Looking at the correlation map in Fig. 6a, a remarkable agreement (R > 0.8) can be

469   seen between SMOS_Reg and SMOSL3 over most of the globe except over some forests

470   areas (e.g., boreal regions) where the correlation values drop below 0.4. Looking at the

471   RMSE map in Fig. 6b, the spatial patterns of the RMSE values are also found to be in

472   correspondence with the vegetation distribution: low RMSE values (~ 0.05 m^3/m^3) are found

473   over areas with low vegetation while high RMSE values are found over moderately vegetated

474   regions.

3.3   SMAP_Reg soil moisture evaluation

This section presents an evaluation of the SMAP_Reg soil moisture product, which was based on applying the LRM algorithm to the SMAP Level 3 TB observations (see Section 2.2.2) and using two soil temperature products: GEOS-5 and ECMWF. Note that the LRM algorithm was calibrated with MERRA-Land soil temperature; here, we only change the input, not the linear regression coefficients, as it will become clear that the temperatures estimated in GEOS-5 and ECMWF do not differ much in the first order. Both these SMAP_Reg soil moisture products were first compared with the SMAP operational Level 3 soil moisture product (SMAP_SCA) to investigate the similarity/dissimilarity between the various SMAP soil moisture products. This was done by computing the R and RMSE statistical criteria between the SMAP_Reg and SMAP_SCA soil moisture products at the global scale. The temporal correlation between SMAP_Reg and SMAP_SCA soil moisture retrievals is shown in Fig. 7a using GEOS-5 and in Fig. 7c using ECMWF. Figs. 7a & c show that the temporal dynamics of both SMAP_Reg and SMAP_SCA soil moisture products are generally very similar with R values larger than 0.8 over most of the globe. However, weaker correlations between SMAP_Reg (ECMWF) and SMAP_SCA (GEOS-5) than between SMAP_Reg (GEOS-5) and SMAP_SCA (GEOS-5) can be seen over a few regions particularly over high latitude areas and Sahara. Fig. 7b shows that the distribution of the RMSE values between SMAP_Reg and SMAP_SCA soil moisture products present clear spatial patterns: low RMSE values over deserts and savannahs (e.g., the Sahara, Australia, Southern Africa, etc.), whereas high values of RMSE values were generally found over vegetated areas. Looking at both Figs. 7a &c (correlations) and Figs. 7b &d (RMSE), there is a general good agreement between SMAP_Reg and SMAP_SCA over regions with low to moderate amounts of vegetation cover.
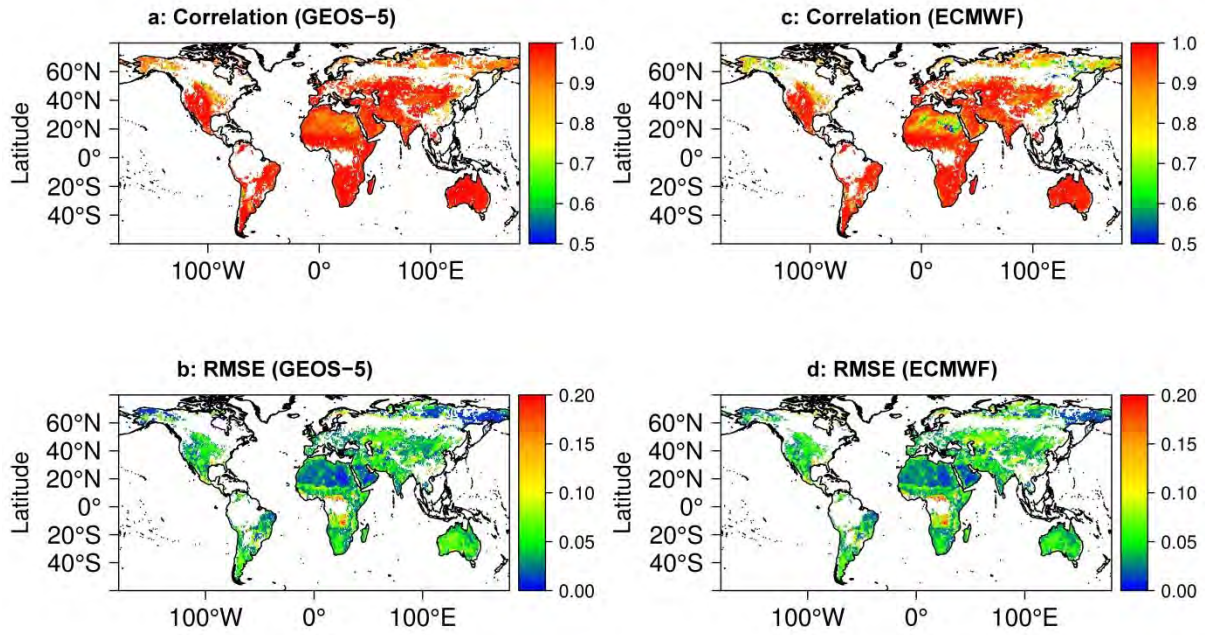
Fig. 7 Comparison between the SMAP-derived soil moisture applying LRM (SMAP_Reg) using two different soil temperature products: GEOS-5 (left) and ECMWF (right) and the SMAP level 3 soil moisture product (SMAP_SCA) from Apr 2015 to Jul 2016: (top) correlation, R (-) and (bottom) RMSE (m^3/m^3).

The SMAP_Reg soil moisture product with GEOS-5 soil temperature as auxiliary

input was additionally evaluated against

    i)   *in situ* soil moisture observations using more than 400 sites from eleven

           networks spread over the globe (see Section 2.1.4); and

    ii)   the operational SMAP and SMOS Level 3 soil moisture products at these

           individual site locations. The SMAP_SCA and the SMOSL3 soil moisture

           products were considered in the evaluation in order to investigate the

           consistency in time variations between the new soil moisture product

           (SMAP_Reg) and the original ones at different sites.

Taylor diagrams (see Section 2.2.3) given in Fig. 8 show the statistics for the sites

individually. Fig. 8 shows values of SDV, R, and the centered RMSE between the remotely

sensed soil moisture products and measured soil moisture values over all sites used in this

26

518   study. In Fig. 8, the performance of SMAP_SCA (blue symbols), SMAP_Reg (red symbols),

519   and SMOSL3 (green symbols) varies from one site to another and from one network to

520   another as demonstrated by the uneven distribution of the sites (shown as circles) in the plots.

521   Looking at the Taylor diagram over the SCAN and SNOTEL sites, the correlations values

522   range between 0 and 0.9 and both SMAP_Reg and SMOSL3 tend to have higher SDV values

523   than SMAP_SCA. Over the REMEDHUS sites, the three algorithms have a comparable

524   performance but with a large variability (as defined by high SDV index) with the *in situ*

525   observations; the correlation values range between 0.4 and 0.8. Over the PBO-H2O sites,

526   SMAP_SCA patterns are closer to the *in situ* patterns than SMOSL3 and SMAP_Reg, which

527   have larger SDV values than the *in situ* observations and most of the correlation values range

528   between 0.5 and 0.9. Over the USCRN sites, the retrieved soil moisture values from all

529   algorithms have a similar variability to that of the *in situ* observations, although SMAP_Reg

530   and SMOSL3 soil moisture products have a larger variability for some sites. Over the RSMN

531   sites, the three products present the same level of performance with respect to the *in situ*

532   observations but all had higher SDV than the *in situ* observations. However, the correlations

533   drop below 0.4 for a few sites for the three products. Over the DAHRA network, the

534   SMOSL3 (best correlation) and SMAP_SCA product lie closest to the observed point

535   followed by SMAP_Reg with higher SDV than the *in situ* observations for all products. Over

536   the iRON sites, the correlations range from 0.4 to 0.8 for the SMOSL3 and SMAP_Reg.

537   SMAP_SCA and SMAP_Reg are comparable in terms of variability and they are closer to the

538   *in situ* patterns than SMOSL3. Over the Oznet network, the three products are comparable in

539   terms of correlations (ranging from 0.6 to 0.9) and, similarly to the RSMN network,

540   overestimate the *in situ* observations. Over the FMI sites, the correlations range from 0.4 to

541   0.8 and 0.9 for SMAP_SCA and SMAP_Reg, respectively. Similarly, to what was obtained

542   over the Oznet sites, the SMAP_SCA and SMAP_Reg products overestimate the *in situ*

27

543   observations over most of the sites. Finally, over SMOSMANIA, SMAP_Reg has better

544   correlations, with *in situ* data ranging from 0.4 to 0.95, than the other two products. For

545   SMOSL3, the correlations drop below 0.4 for a few sites. Overall, all three products have

546   approximately the same level of performance in terms of variability but SMAP_SCA is

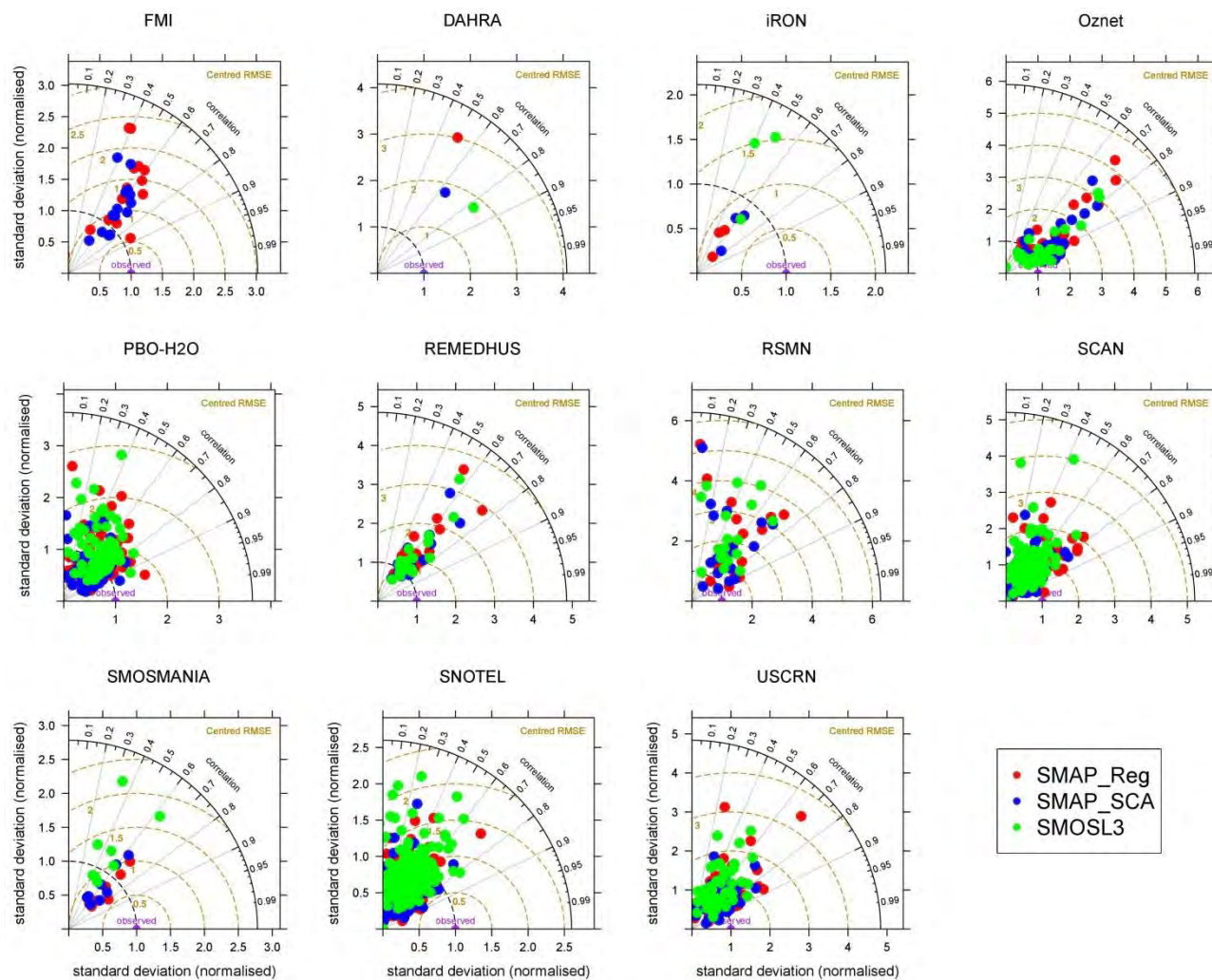547   slightly better in terms of temporal dynamics.

548

549

Fig. 8 Taylor's diagrams for SMAP_Reg (in red), SMAP_SCA (in blue), and SMOSL3 (in green) over the FMI, DAHRA, iRON, and Oznet (upper panel), over SCAN, PBO-H2O, REMEDHUS, and RSMN sites (middle panel), and over SNOTEL, USCRN, and SMOSMANIA sites (lower panel).

554   In order to have a general idea on the overall performance of SMAP_SCA,

555   SMAP_Reg, and SMOSL3, the average of the Bias, RMSE, and UnbRMSE values and the

556   median of the correlation values for all sites were computed per each network. Given the

557   different sizes of the networks, the varying sample sizes, and varying temporal and spatial

558   autocorrelations, the values are only indicative and no statistical confidence levels are

559   provided. It should be noted that the average and median values were only computed when

560   the site has a number of observations > 15 and p-value <0.05. This is presented in Table 2

561   and Fig. 9, which show the comparison statistics for the three algorithms i.e. SMAP_Reg,

562   SMAP_SCA, and SMOSL3 against the *in situ* observations. It can be seen in Table 2 and Fig.

563   9 that the best R scores (R > 0.80) for the three algorithms were obtained over the Oznet sites

564   while the worst ones were observed over (R ~ 0.58) over the SNOTEL sites for SMAP_SCA

565   and over the DAHRA and SMOSMANIA sites (R=0.51 and R=0.45 for SMAP_Reg and

566   SMOSL3 respectively). SMOSL3 had highest R values over the DAHRA site while

567   SMAP_Reg had highest R values over SMOSMANIA. Other than those two networks,

568   SMAP_SCA had highest R values. However, both SMAP products i.e. SMAP_SCA and

569   SMAP_Reg have comparable performance particularly in terms of correlation coefficients. In

570   terms of unbRMSE, SMAP_SCA had lower values for all sites except in Oznet where the

571   lowest values were obtained by SMOSL3. Even though it is difficult to compare absolute

572   values at *in situ* locations, a comparison based on a large sample can give some indication of

573   biases: the Bias values showed that all products are generally dry, except over RSMN,

574   DAHRA, and Oznet (and FMI for SMAP_SCA). Unlike SMAP_Reg, a notable overall

575   positive bias is obtained over FMI for SMAP_SCA (overestimation). The overestimation of

576   *in situ* soil moisture observations over RSMN and FMI networks by SMAP_SCA is in line

577   with the recent findings of Zeng et al. (2016).

578

579

580
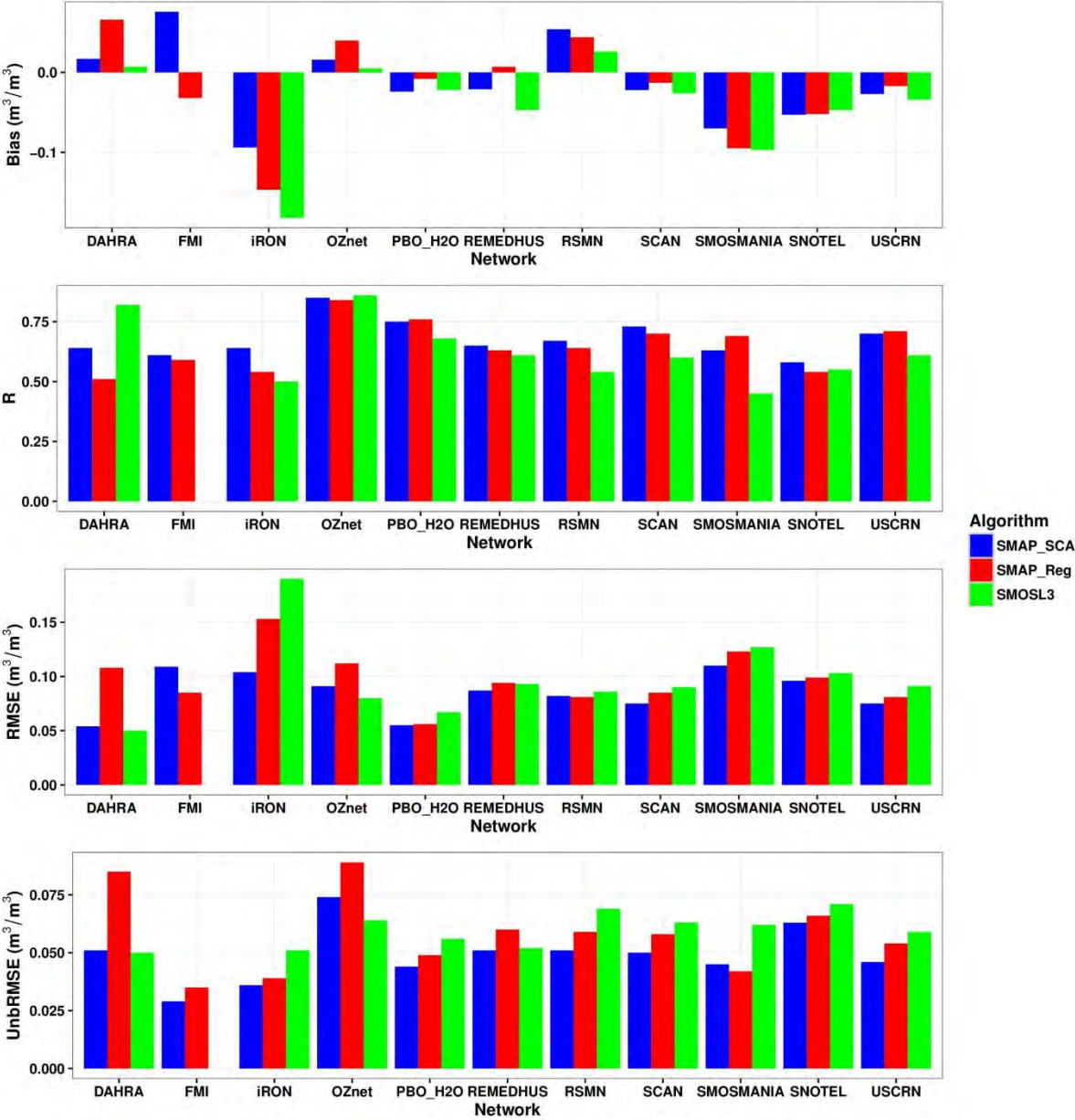
Fig. 9 Bar charts showing Bias (m³/m³), R, RMSE (m³/m³), and UnbRMSE (m³/m³) between SMAP_SCA (in blue), SMAP_Reg (in red), and SMOSL3 (in green) and the observed soil moisture over the 11 networks used in this study.

584 **Table 2** Statistics of the evaluation of the SMAP_Reg, SMAP_SCA, and SMOSL3 against ground based measurements. The average (median
585 for R instead of "average" as correlation is not additive) values were only computed for sites that have p_value < 0.05 and number of
586 observations was higher than 15.

Matric / Algorithm Network (No of sites)	Bias (m^3/m^3) (mean)			RMSE (m^3/m^3) (mean)			R (median)			UnbRMSE (m^3/m^3) (mean)		
	SMAP_SCA	SMAP_Reg	SMOS L3	SMAP_SCA	SMAP_Reg	SMOS L3	SMAP_SCA	SMAP_Reg	SMOS L3	SMAP_SCA	SMAP_Reg	SMOS L3
REMEDHUS (19)	-0.021	**0.007**	-0.047	**0.087**	0.094	0.093	**0.65**	0.63	0.61	**0.051**	0.060	0.052
PBO_H2O (76)	-0.024	**-0.008**	-0.022	**0.055**	0.056	0.067	0.75	**0.76**	0.68	**0.044**	0.049	0.056
RSMN (16)	0.054	0.044	**0.026**	0.082	**0.081**	0.086	**0.67**	0.64	0.54	**0.051**	0.059	0.069
SCAN (104)	-0.022	**-0.013**	-0.026	**0.075**	0.085	0.090	**0.73**	0.70	0.60	**0.050**	0.058	0.063
SNOTEL (125)	-0.053	-0.052	**-0.047**	**0.096**	0.099	0.103	**0.58**	0.54	0.55	**0.063**	0.066	0.071
USCRN (51)	-0.027	**-0.017**	-0.034	**0.075**	0.081	0.091	0.70	**0.71**	0.61	**0.046**	0.054	0.059
FMI (14)	0.076	**-0.032**	-	0.109	**0.085**	-	**0.61**	0.59	-	**0.029**	0.035	-
iRON (3)	**-0.094**	-0.147	-0.182	**0.104**	0.153	0.190	**0.64**	0.54	0.50	**0.036**	0.039	0.051
DAHRA (1)	0.017	0.066	**0.007**	0.054	0.108	**0.050**	0.64	0.51	**0.82**	0.051	0.085	**0.050**
SMOSMANIA (7)	**-0.070**	-0.095	-0.097	**0.110**	0.123	0.127	0.63	**0.69**	0.45	0.045	**0.042**	0.062
Oznet (34)	0.016	0.040	**0.005**	0.091	0.112	**0.080**	0.85	0.84	**0.86**	0.074	0.089	**0.064**

587

4   Discussion

We investigated the potential utility of a physically based multi-linear regression approach to retrieve soil moisture from two microwave remote sensing satellites that operate at L-band: SMOS and SMAP. The approach consists of two steps:

(i)   a calibration step to compute regression coefficients using SMOS TB and soil moisture over 2013-2014 (calibration period); and

(ii)   a production step to retrieve soil moisture from SMAP TB using the computed regression coefficients, for Apr 2015 to Jul 2016 (production period).

4.1   SMAP and SMOS inter-comparison

Before applying the regressions, an inter-comparison was made between SMOS and SMAP TBs and soil moisture. From the results (Fig. 3 & 4), it was shown that there is a very good agreement between the two datasets. However, small discrepancies (2 to 4 K of Bias) between the SMOS and SMAP TBs were found over most of the globe and high discrepancies were found particularly over regions affected by RFI (Western Europe, North Africa, etc.). This is not unexpected due to the fact that, as indicated in Section 2.1.1 and 2.1.2, the SMOSL3 TB product provides TBs on top of the atmosphere and there is no correction for sky and atmosphere contributions whereas SMAP TB is provided at the surface. According to De Lannoy et al. (2015), a difference of less than 2 K for H-Pol TB and 1 K for V-Pol TB at $40°$ incidence angle between SMOS TB and SMAP TB can be attributed to the contributions of the atmospheric and reflected sky (e.g., cosmic and galactic) radiations. This low difference can be explained by the fact that the effects of (i) the contribution of the atmosphere to TB (direct and reflected) and (ii) the attenuation effects due to the atmosphere, partially offset each other. Nevertheless, local and short-term values regularly exceed 5 K (De Lannoy et al., 2015). In addition, SMAP TBs are water-body

33

613 corrected while SMOS TBs are not. Thus, the SMOS and SMAP TBs do not correspond

614 exactly to the same pixel coverage: the SMOS TBs correspond to the whole pixel, while the

615 SMAP TBs correspond to the whole pixel, but excluding open water areas. As the emission

616 of open water surfaces (~ 60 – 150 k) is small in comparison to the emission of soil and

617 vegetation-covered surfaces, applying this correction leads systematically to an increase in

618 the TBs values. Note that for pixels with a fraction of water bodies higher than 10%, data

619 were filtered out. But even after this filtering, the water TB correction may have an impact on

620 the TB values. This water TB correction may explain the warm "Bias" (~10 K) of the SMAP

621 TBs with respect to the SMOS TBs over high latitude and boreal regions (where many pixels

622 may contain lakes, rivers, wetlands, etc.). Excluding these regions, a small cold bias of

623 SMAP TBs with respect to SMOS TBs can be noted (~3-6 K). Overall, a very good

624 agreement was found globally between the SMAP and SMOS TBs data.

625 **4.2   Regression calibration and soil moisture production**

626   The regression model was run for each land cover category (defined here using the

627 IGBP land cover map) separately and thus we obtained coefficients of each land cover

628 category. These values vary from one land cover category to another, reflecting the different

629 characteristics for each land cover category. These three parameters as indicated by Saleh et

630 al. (2006) are a function of the soil type and roughness. The regression approach quality was

631 evaluated in two ways:

632   (i)   first, we estimated soil moisture from SMOS TB and compared the predicted

633   soil moisture (SMOS_Reg) to the reference (SMOSL3) using correlation and

634   RMSE, over the calibration period (2013-2014). High correlations (R> 0.8) and

635   low RMSE values were obtained between SMOS_Reg and the reference over

636   the continental surfaces, indicating that the spatio-temporal dynamics of

637   SMOSL3 was well captured by SMOS_Reg. However, some differences can be

638   noted in terms of magnitude over high to moderate vegetation areas and high

639   latitude regions. This is not unexpected due to uncertainties in the SMOS

640   datasets caused by the high vegetation attenuation effects in these regions,

641   which is a major problem for most of the remotely sensed soil moisture

642   retrievals (Vittucci et al., 2016; Wigneron et al., 2003); and

643   (ii)   Second, we estimated soil moisture from SMAP TB for the Apr 2015 to Jul

644   2016 period (SMAP-Reg) and compared it to the original SMAP_SCA and the

645   SMOSL3 soil moisture products against more than 400 sites over the world.

646   Soil temperature is an important input in the radiative transfer equation and has a

647 significant impact on the final estimate of the soil moisture retrievals (Holmes et al., 2012;

648 Lv et al., 2016; Parinussa et al., 2011). In order to study how sensitive is the retrieved soil

649 moisture to the soil temperature effects, we used soil temperature from two different

650 sources: ECMWF and GEOS-5. We applied the regression coefficients to SMAP TB using

651 these two products and then we compared with SMAP_SCA. It was found that in general

652 the spatial patterns are similar for both products in terms of R and RMSE values; however,

653 the correlations between SMAP_Reg (ECMWF) and SMAP_SCA (GEOS-5) are lower than

654 the correlations between SMAP_Reg (GEOS-5) and SMAP_SCA (GEOS-5) over some

655 regions (e.g., Sahara, Far Eastern Federal District, East-Central Canada, etc.). The better

656 agreement between SMAP_Reg (GEOS-5) and SMAP_SCA (GEOS-5) does not necessarily

657 mean that the quality of GEOS-5 is better than ECMWF. This could simply results from the

658 fact that the same soil temperature product was used in both the regression approach and the

659 SMAP_SCA algorithm. However, it does seem that soil temperature has an important

660 impact on the soil moisture retrievals (e.g., Lv et al., 2016), i.e. using the same soil

661 temperature leads to similar soil moisture retrievals from SMAP no matter if different

662   retrieval approaches are used. This could partially explain the strong agreement found

663   between SMAP_SCA and SMAP_Reg.

664   Results from the comparison between SMAP_Reg both (ECMWF & GEOS-5) and

665   SMAP_SCA showed that SMAP_Reg is in agreement with SMAP_SCA, particularly in

666   terms of temporal dynamics which is of high relevance (Crow et al., 2010; Liu et al., 2012).

667   Moreover, it is noticed here that the performance of the "production" step i.e. comparison

668   between SMAP_Reg and SMAP_SCA is much better than the "calibration" step i.e.

669   comparison between SMOS_Reg and SMOSL3. This can be partly explained by three

670   reasons:

671   1-   in the calibration step, the TBs used are not exactly the same while in the

672   production step they are. More specifically, the SMOSL3 soil moisture product is not

673   directly retrieved from SMOSL3 TB but from TB products in the Fourier domain (L1B);

674   thus the TB used in the regression does not necessarily match the actual TB used to retrieve

675   SMOSL3 soil moisture. Therefore it is expected that the temporal dynamics of the two soil

676   moisture products will be more similar because they will be driven by the common input

677   TB dynamics. This uncertainty, among others, may affect the quality of the calibration;

678   2-   the quality of SMAP TB seems to be very good and therefore whatever the

679   used algorithm, the resultant soil moisture is the same particularly in terms of temporal

680   dynamics. This, again, may partially explain the strong similarity between the two products

681   i.e. SMAP_Reg and SMAP_SCA; and

682   3-   the regression (LRM coefficients) is based on MERRA-Land T_G, which is

683   similar to the GEOS-5 product used in SMAP_SCA and not in SMOSL3 (for which the

684   ECMWF product is used); explicitly indicating that soil temperature may play a crucial role

685   in the quality of the SM retrievals.

686

36

687 **4.3 SMAP_Reg soil moisture evaluation**

688 Results from evaluating both SMAP products and SMOSL3 against *in situ*

689 observations showed that SMAP_SCA and SMAP_Reg soil moisture products have

690 comparable performance with similar R values over the REMEDHUS, PBO_H2O,

691 SNOTEL, SCAN, Oznet, and USCRN sites. Nevertheless, all three remotely sensed soil

692 moisture products had poor performance over the SNOTEL. The poor performance of the

693 three algorithms over the SNOTEL network can be attributed to several reasons: among

694 them it should be considered that most of the SNOTEL sites are located in mountain regions

695 with forests and freezing and thawing processes, more details on these aspects can be found

696 in Al Bitar et al. (2012). It should be kept in mind that when using only the recommended

697 retrievals for SMAP, there was no data left from the iRON sites. So the statistics for this

698 particular network were based on data without considering if the retrieval was

699 recommended or not but other filters were, however, applied.

700 All remotely sensed soil moisture products underestimated generally the *in situ*

701 observations used in this study. The bias values ranged from -0.095 m^3/m^3 (SMOSMANIA)

702 to 0.066 m^3/m^3 (DAHRA) for SMAP_Reg, from -0.094 m^3/m^3 (iRON) to 0.076 m^3/m^3 (FMI)

703 for SMAP_SCA, and from -0.182 m^3/m^3 (iRON) to 0.026 m^3/m^3 (RSMN) for SMOSL3. This

704 so-called "dry" bias of SMOSL3 and SMAP_SCA is in line with previous studies (Al-Yaari

705 et al., 2014b; Al Bitar et al., 2012; Chan et al., 2016; Dente et al., 2012). On the other hand,

706 an overestimation was found over FMI (for only SMAP_SCA) and RSMN, DAHRA, and

707 Oznet sites (for the three products). It should be kept in mind that FMI is a very specific

708 network: the sites of FMI are located in high latitude regions with cold climate in which

709 remotely-send soil moisture retrievals are influenced by the effects of soil freezing and

710 thawing processes, organic matter in the soil substrate and the presence of numerous water

711 bodies and bogs (Rautiainen et al., 2012; Zeng et al., 2016). The reasoning behind the

37

712 underestimation/overestimation of the *in situ* soil moisture values is a challenge. The dry bias

713 could be related to the different spatial scales and sampling depths between the satellites and

714 the *in situ* observations (e.g., Dorigo et al., 2015; Escorihuela et al., 2010; Rondinelli et al.,

715 2015). Moreover, although RFI was severely filtered from the SMOS datasets, it could be

716 that some sources of RFI are still not filtered/detected, which can explain the rather general

717 underestimation which is found in this study (Oliva et al., 2016). This was evident especially

718 for SMOS as seen in Fig. 3 where SMOS still has higher TBs close to those regions despite

719 filtering RFI. The reader is referred to Al Bitar et al. (2012) for a discussion on these

720 questions.

721   In terms of UnbRMSE, a comparable performance between SMAP_SCA and

722 SMAP_Reg was found over the SMOSMANIA, iRON, and SNOTEL sites but lower values

723 were obtained with SMAP_SCA over the other networks. SMOSL3 had generally higher

724 UnbRMSE values than both SMAP_SCA and SMAP_Reg. However, SMOSL3 had lower

725 values over the Oznet and DAHRA sites.

726   It was noted from Table 2 and Fig. 9, that the SMAP TB-based soil moisture products

727 (SMAP_SCA and SMAP_Reg) have a slightly better performance than SMOSL3 for most of

728 the networks especially in terms of temporal dynamics. Although the three algorithms use TB

729 at L-band and rely on the same radiative transfer equation (tau-omega model), they vary in

730 many things (e.g., ancillary datasets, model parameterizations and assumptions). For instance,

731 SMOS and SMAP use two different land cover maps: ECOCLIMAP 2004 (containing 213

732 classes) for SMOS and MODIS IGBP (containing 17 classes) for SMAP, so it is likely there

733 is a mismatch between the real land cover and the theoretical land cover used in SMAP and

734 SMOS soil moisture retrievals leading to a different behavior of the soil moisture retrievals.

735 This may also partially explain the similarity between SMAP_Reg and SMAP_SCA given

736 the use of the same land cover. These differences were already noted in the direct inter-

comparison between SMOSL3 and SMAP_SCA displayed in Fig. 4. The SMOS team is currently investigating the impact of land cover mapping and the possibility to replace the ECOCLIMAP map by the IGBP map in the SMOS soil moisture retrieval algorithm. Furthermore, the better performance of SMAP soil moisture products could be related to the enhanced quality of the SMAP TB observations due to an improved RFI mitigation and detection system (Piepmeier et al., 2016). Moreover, SMOS TB observations have a radiometric error of ~ 3 to 3.5 K while SMAP TB observations have a radiometric error of ~ 1 K (De Lannoy et al., 2015). Finally, SMOS and SMAP use different surface soil temperature sources for their operational products.

Based on the presented results, it can be noted that applying regression analysis to TB (from SMAP and SMOS) observed at L-band (1.4 GHz) gave better results compared to what was found by Al-Yaari et al. (2016), who applied the LRM algorithm to TB observed at C-band (from AMSR-E; 6.9 GHz). This is not unexpected, as the simplifications and assumptions (e.g., neglecting the scattering effects) of the LRM method are more valid at L-band. Moreover, both SMAP and SMOS observe TB at the same frequency i.e. L-band, which is considered optimal for soil moisture retrievals (Chan et al., 2016; Jackson, 1993). On the other hand, a similar behavior with Al-Yaari et al. (2016) of the regression coefficients that correspond to the H polarization and V polarization was found: low (high) coefficient values at H polarization correspond generally to high (low) values at V polarization over most of the regions.

5   Conclusions

760

761   This study demonstrated the potential benefits of combining SMOS and SMAP

762   datasets given the good performance of SMAP_Reg compared to SMOSL3 and SMAP_SCA

763   original products over some regions. This in return shows the close similarity between SMOS

764   and SMAP TB observations and highlights that an integration of SMAP and SMOS data sets

765   to build a long term soil moisture record will be successful and higher temporal frequency.

766   Finally, this first evaluation of preliminary SMAP products, and the inter-comparison with

767   SMOS datasets provided insights and statistics that can be useful for SMAP/SMOS soil

768   moisture product validation and SMAP/SMOS algorithm refinements and convergence on

769   auxiliary data sets. A calibration of the soil and vegetation effects has been recently made

770   (Fernández Morán et al., 2016). A new SMOS Level 3 soil moisture product integrating this

771   new calibration and with a significantly improved accuracy is being produced. Future

772   research will consider the calibration of SMAP-Reg with this new SMOS product and further

773   fusion studies will be continued by applying LRM to the SMOS and SMAP datasets

774   considering other important variables such as the vegetation opacity.

775

782

783

784

785   **References**

786   Aires, F., Aznay, O., Prigent, C., Paul, M. & Bernardo, F. (2012). Synergistic multi-
787   wavelength remote sensing versus a posteriori combination of retrieved products:
788   Application for the retrieval of atmospheric profiles using MetOp-A. *Journal of*
789   *Geophysical Research: Atmospheres, 117*

790   Al-Yaari, A., Wigneron, J.P., Ducharne, A., Kerr, Y.H., Wagner, W., De Lannoy, G.,
791   Reichle, R., Al Bitar, A., Dorigo, W., Richaume, P. & Mialon, A. (2014a). Global-
792   scale comparison of passive (SMOS) and active (ASCAT) satellite based microwave
793   soil moisture retrievals with soil moisture simulations (MERRA-Land). *Remote*
794   *Sensing of Environment, 152*, 614-626

795   Al-Yaari, A., Wigneron, J.P., Ducharne, A., Kerr, Y., de Rosnay, P., de Jeu, R., Govind, A.,
796   Al Bitar, A., Albergel, C., Muñoz-Sabater, J., Richaume, P. & Mialon, A. (2014b).
797   Global-scale evaluation of two satellite-based passive microwave soil moisture
798   datasets (SMOS and AMSR-E) with respect to Land Data Assimilation System
799   estimates. *Remote Sensing of Environment, 149*, 181-195

800   Al-Yaari, A., Wigneron, J.P., Kerr, Y., de Jeu, R., Rodriguez-Fernandez, N., van der Schalie,
801   R., Al Bitar, A., Mialon, A., Richaume, P., Dolman, A. & Ducharne, A. (2016).
802   Testing regression equations to derive long-term global soil moisture datasets from
803   passive microwave observations. *Remote Sensing of Environment, 180*, 453-464

804   Al Bitar, A., Leroux, D., Kerr, Y.H., Merlin, O., Richaume, P., Sahoo, A. & Wood, E.F.
805   (2012). Evaluation of SMOS Soil Moisture Products Over Continental U.S. Using the
806   SCAN/SNOTEL Network. *IEEE Transactions on Geoscience and Remote Sensing,*
807   *50*, 1572-1586

808   Albergel, C., Rüdiger, C., Pellarin, T., Calvet, J.-C., Fritz, N., Froissard, F., Suquia, D.,
809   Petitpa, A., Piguet, B. & Martin, E. (2008). From near-surface to root-zone soil

41

810   moisture using an exponential filter: an assessment of the method based on in-situ

811   observations and model simulations. *Hydrology and Earth System Sciences*

812   *Discussions, 12*, 1323-1337

813   Balsamo, G., Viterbo, P., Beljaars, A.C.M., van den Hurk, B.J.J.M., Hirschi, M., Betts, A.K.

814   & K., S. (2009). A revised hydrology for the ECMWF model: Verification from field

815   site to terrestrial water storage and impact in the ECMWF-IFS. *J. Hydrometeor, 10*

816   Bartalis, Z., Hasenauer, S., Naeimi, V. & Wagner, W. (2007). WARP-NRT 2.0 Reference

817   Manual. ASCAT Soil Moisture Report Series, No. 14. *Institute of Photogrammetry*

818   *and Remote Sensing, Vienna University of Technology, Austria*

819   Bell, J.E., Palecki, M.A., Baker, C.B., Collins, W.G., Lawrimore, J.H., Leeper, R.D., Hall,

820   M.E., Kochendorfer, J., Meyers, T.P., Wilson, T. & Diamond, H.J. (2013). U.S.

821   Climate Reference Network Soil Moisture and Temperature Observations. *Journal of*

822   *Hydrometeorology, 14*, 977-988

823   Berg, A., Lintner, B.R., Findell, K.L., Malyshev, S., Loikith, P.C. & Gentine, P. (2014).

824   Impact of Soil Moisture–Atmosphere Interactions on Surface Temperature

825   Distribution. *Journal of Climate, 27*, 7976-7993

826   Berrisford, P., Dee, D., Poli, P., Brugge, R., Fielding, K., Fuentes, M., Kallberg, P.,

827   Kobayashi, S., Uppala, S. & Simmons, A. (2011). The ERA-Interim archive Version

828   2.0, ERA Report Series 1, ECMWF, Shinfield Park. *Reading, UK, 13177*

829   Calvet, J.-C., Fritz, N., Froissard, F., Suquia, D., Petitpa, A. & Piguet, B. (2007). In situ soil

830   moisture observations for the CAL/VAL of SMOS: The SMOSMANIA network. In,

831   *Geoscience and Remote Sensing Symposium, 2007. IGARSS 2007. IEEE International*

832   (pp. 1196-1199): IEEE

833   Chan, S., Rajat Bindlish, Peggy O'Neill, Eni Njoku, Tom Jackson, Andreas Colliander, Fan

834   Chen, Mariko Burgin, Scott Dunbar, Jeffrey Piepmeier, Simon Yueh, Dara Entekhabi,

835   Michael H. Cosh, Todd Caldwell, Jeffrey Walker, Xiaoling Wu, Aaron Berg, Tracy

836   Rowlandson, Anna Pacheco, Heather McNairn, Marc Thibeault, José Martínez-

837   Fernández, Ángel González-Zamora, Mark Seyfried, David Bosch, Patrick Starks,

838   David Goodrich, John Prueger, Michael Palecki, Eric E. Small, Marek Zreda, Jean-

839   Christophe Calvet, Wade T. Crow & Kerr, Y. (2016). Assessment of the SMAP

840   Passive Soil Moisture Product. *IEEE Transactions on Geoscience and Remote*

841   *Sensing, 54*, 4994 - 5007

842 Chen, T., McVicar, R.T., Wang, G., Chen, X., de Jeu, A.R., Liu, Y.Y., Shen, H., Zhang, F. &

843   Dolman, J.A. (2016). Advantages of Using Microwave Satellite Soil Moisture over

844   Gridded Precipitation Products and Land Surface Model Output in Assessing

845   Regional Vegetation Water Availability and Growth Dynamics for a Lateral Inflow

846   Receiving Landscape. *Remote Sensing, 8*

847 Choudhury, B.J., Schmugge, T.J., Chang, A. & Newton, R.W. (1979). Effect of surface

848   roughness on the microwave emission from soils. *Journal of Geophysical Research:*

849   *Oceans, 84*, 5699-5706

850 Crow, W.T., Miralles, D.G. & Cosh, M.H. (2010). A Quasi-Global Evaluation System for

851   Satellite-Based Surface Soil Moisture Retrievals. *IEEE Transactions on Geoscience*

852   *and Remote Sensing, 48*, 2516-2527

853 De Lannoy, G.J.M., Reichle, R.H., Peng, J., Kerr, Y., Castro, R., Kim, E.J. & Liu, Q. (2015).

854   Converting Between SMOS and SMAP Level-1 Brightness Temperature

855   Observations Over Nonfrozen Land. *IEEE Geoscience and remote sensing letters, 12*,

856   1908-1912

857 De Lannoy, G.J.M. & Reichle, R.H. (2015). Global Assimilation of Multiangle and

858   Multipolarization SMOS Brightness Temperature Observations into the GEOS-5

859   Catchment Land Surface Model for Soil Moisture Estimation. *Journal of*

860   *Hydrometeorology, 17*, 669-691

861   Dente, L., Su, Z. & Wen, J. (2012). Validation of SMOS Soil Moisture Products over the

862   Maqu and Twente Regions. *Sensors, 12*, 9965-9986

863   Dorigo, W.A., Wagner, W., Hohensinn, R., Hahn, S., Paulik, C., Xaver, A., Gruber, A.,

864   Drusch, M., Mecklenburg, S., van Oevelen, P., Robock, A. & Jackson, T. (2011). The

865   International Soil Moisture Network: a data hosting facility for global in situ soil

866   moisture measurements. *Hydrol. Earth Syst. Sci., 15*, 1675-1698

867   Dorigo, W.A., Xaver, A., Vreugdenhil, M., Gruber, A., Hegyiová, A., Sanchis-Dufau, A.D.,

868   Zamojski, D., Cordes, C., Wagner, W. & Drusch, M. (2013). Global Automated

869   Quality Control of In Situ Soil Moisture Data from the International Soil Moisture

870   Network. *Vadose Zone Journal, 12*

871   Dorigo, W.A., Gruber, A., De Jeu, R.A.M., Wagner, W., Stacke, T., Loew, A., Albergel, C.,

872   Brocca, L., Chung, D., Parinussa, R.M. & Kidd, R. (2015). Evaluation of the ESA

873   CCI soil moisture product using ground-based observations. *Remote Sensing of*

874   *Environment, 162*, 380-395

875   Enenkel, M., Reimer, C., Dorigo, W., Wagner, W., Pfeil, I., Parinussa, R. & De Jeu, R.

876   (2015). Combining satellite observations to develop a daily global soil moisture

877   product for a wide range of applications. *Hydrol. Earth Syst. Sci. Discuss., 2015*,

878   11549-11589

879   Entekhabi, D., Njoku, E.G., O'Neill, P.E., Kellogg, K.H., Crow, W.T., Edelstein, W.N.,

880   Entin, J.K., Goodman, S.D., Jackson, T.J., Johnson, J., Kimball, J., Piepmeier, J.R.,

881   Koster, R.D., Martin, N., McDonald, K.C., Moghaddam, M., Moran, S., Reichle, R.,

882   Shi, J.C., Spencer, M.W., Thurman, S.W., Leung, T. & Van Zyl, J. (2010). The Soil

883   Moisture Active Passive (SMAP) Mission. *Proceedings of the IEEE, 98*, 704-716

884 Escorihuela, M.J., Chanzy, A., Wigneron, J.P. & Kerr, Y.H. (2010). Effective soil moisture

885   sampling depth of L-band radiometry: A case study. *Remote Sensing of Environment,*

886   *114*, 995-1001

887 Fernández Morán, R., Wigneron, J.-P., De Lannoy, G., Lopez-Baeza, E., Mialon, A.,

888   Mamoodi, A., Parrens, M., Al Bitar, A., Richaume, P. & Kerr, Y. (2016). Calibrating

889   the effective scattering albedo in the SMOS algorithm: some first results. *2016 IEEE*

890   *International Geoscience and Remote Sensing Symposium (IGARSS), Beijing, 2016*

891 Friedl, M.A., Sulla-Menashe, D., Tan, B., Schneider, A., Ramankutty, N., Sibley, A. &

892   Huang, X. (2010). MODIS Collection 5 global land cover: Algorithm refinements and

893   characterization of new datasets. *Remote Sensing of Environment, 114*, 168-182

894 GCOS (2010). Implementation Plan for the Global Observing System for Climate in Support

895   of the UNFCC (2010 Update)

896 Grant, J.P., Saleh-Contell, K., Wigneron, J.P., Guglielmetti, M., Kerr, Y.H., Schwank, M.,

897   Skou, N. & Griend, A.A.V.d. (2008). Calibration of the L-MEB Model Over a

898   Coniferous and a Deciduous Forest. *IEEE Transactions on Geoscience and Remote*

899   *Sensing, 46*, 808-818

900 Hirschi, M., Mueller, B., Dorigo, W. & Seneviratne, S.I. (2014). Using remotely sensed soil

901   moisture for land–atmosphere coupling diagnostics: The role of surface vs. root-zone

902   soil moisture variability. *Remote Sensing of Environment, 154*, 246-252

903 Holmes, T.R.H., de Rosnay, P., de Jeu, R., Wigneron, R.J.P., Kerr, Y., Calvet, J.C.,

904   Escorihuela, M.J., Saleh, K. & Lemaître, F. (2006). A new parameterization of the

905   effective temperature for L band radiometry. *Geophysical Research Letters, 33*

906 Holmes, T.R.H., Jackson, T.J., Reichle, R.H. & Basara, J.B. (2012). An assessment of surface

907   soil temperature products from numerical weather prediction models using ground-

908   based measurements. *Water Resources Research, 48*

Hupet, F. & Vanclooster, M. (2002). Intraseasonal dynamics of soil moisture variability within a small agricultural maize cropped field. *Journal of Hydrology, 261*, 86-101

Jackson, T.J. & Schmugge, T.J. (1991). Vegetation effects on the microwave emission of soils. *Remote Sensing of Environment, 36*, 203-212

Jackson, T.J. (1993). Measuring surface soil moisture using passive microwave remote sensing. *Hydrol. Process, 7*, 139-152

Jackson, T.J., O'Neill, P., Njoku, E., S, C., Bindlish, R., Colliander, A., Chen, F., Burgin, M., S.Dunbar, Piepmeier, J., Cosh, M., Caldwell, T., Walker, J., Wu, X., Berg, A., Rowlandson, T., A.Pacheco, McNairn, H., Thibeault, M., Martínez-Fernández, J., González-Zamora, Á., M. Seyfried, D.Bosch, P. Starks, D. Goodrich, J. Prueger, Z. Su, R. van der Velde, J. Asanuma, M. Palecki, E. Small, M. Zreda, J. Calvet, W. Crow, Y. Kerr, Yueh, S. & Entekhabi, D. (2016). Soil Moisture Active Passive (SMAP) Project Calibration and Validation for the L2/3_SM_P Version 3 Data Products. *SMAP Project, JPL D-93720 Jet Propulsion Laboratory, Pasadena, CA*

Kerr, Y. (2007). Soil moisture from space: Where are we? *Hydrogeology Journal, 15*, 117-120

Kerr, Y., Jacquette, E., Al Bitar, A., Cabot, F., Mialon, A., Richaume , P., Quesney, A., Berthon, L. & Wigneron, J. (2013). The CATDS SMOS L3 soil moisture retrieval processor, Algorithm Theoretical Baseline Document (ATBD). *SO-TN-CBSA-GS-0029*

Kerr, Y.H., Waldteufel, P., Wigneron, J.P., Martinuzzi, J., Font, J. & Berger, M. (2001). Soil moisture retrieval from space: the Soil Moisture and Ocean Salinity (SMOS) mission. *IEEE Transactions on Geoscience and Remote Sensing, 39*, 1729-1735

Kerr, Y.H., Waldteufel, P., Wigneron, J.P., Delwart, S., Cabot, F., Boutin, J., Escorihuela, M.J., Font, J., Reul, N., Gruhier, C., Juglea, S.E., Drinkwater, M.R., Hahne, A.,

934   Martin-Neira, M. & Mecklenburg, S. (2010). The SMOS Mission: New Tool for

935   Monitoring Key Elements ofthe Global Water Cycle. *Proceedings of the IEEE, 98*,

936   666-687

937 Kerr, Y.H., Waldteufel, P., Richaume, P., Wigneron, J.P., Ferrazzoli, P., Mahmoodi, A., Al

938   Bitar, A., Cabot, F., Gruhier, C., Juglea, S.E., Leroux, D., Mialon, A. & Delwart, S.

939   (2012). The SMOS Soil Moisture Retrieval Algorithm. *IEEE Transactions on*

940   *Geoscience and Remote Sensing, 50*, 1384-1403

941 Kerr, Y.H., Al-Yaari, A., Rodriguez-Fernandez, N., Parrens, M., Molero, B., Leroux, D.,

942   Bircher, S., Mahmoodi, A., Mialon, A., Richaume, P., Delwart, S., Al Bitar, A.,

943   Pellarin, T., Bindlish, R., Jackson, T.J., Rüdiger, C., Waldteufel, P., Mecklenburg, S.

944   & Wigneron, J.P. (2016). Overview of SMOS performance in terms of global soil

945   moisture monitoring after six years in operation. *Remote Sensing of Environment,*

946   *180*, 40-63

947 Kolassa, J., Aires, F., Polcher, J., Prigent, C., Jimenez, C. & Pereira, J.M. (2013). Soil

948   moisture retrieval from multi-instrument observations: Information content analysis

949   and retrieval methodology. *Journal of Geophysical Research: Atmospheres, 118*,

950   4847-4859

951 Larson, K.M., Small, E.E., Gutmann, E.D., Bilich, A.L., Braun, J.J. & Zavorotny, V.U.

952   (2008). Use of GPS receivers as a soil moisture network for water cycle studies.

953   *Geophysical Research Letters, 35*, n/a-n/a

954 Liu, Y.Y., Dorigo, W.A., Parinussa, R.M., de Jeu, R.A.M., Wagner, W., McCabe, M.F.,

955   Evans, J.P. & van Dijk, A.I.J.M. (2012). Trend-preserving blending of passive and

956   active microwave soil moisture retrievals. *Remote Sensing of Environment, 123*, 280-

957   297

958 Lv, S., Zeng, Y., Wen, J. & Su, Z. (2016). A reappraisal of global soil effective temperature

959   schemes. *Remote Sensing of Environment, 183*, 144-153

960 Mo, T., Choudhury, B.J., Schmugge, T.J., Wang, J.R. & Jackson, T.J. (1982). A model for

961   microwave emission from vegetation-covered fields. *Journal of Geophysical*

962   *Research: Oceans, 87*, 11229-11237

963 Njoku, E.G. & Li, L. (1999). Retrieval of land surface parameters using passive microwave

964   measurements at 6-18 GHz. *IEEE Transactions on Geoscience and Remote Sensing,*

965   *37*, 79-93

966 Njoku, E.G., Wilson, W.J., Yueh, S.H., Dinardo, S.J., Fuk, K.L., Jackson, T.J., Lakshmi, V.

967   & Bolten, J. (2002). Observations of soil moisture using a passive and active low-

968   frequency microwave airborne sensor during SGP99. *IEEE Transactions on*

969   *Geoscience and Remote Sensing, 40*, 2659-2673

970 Njoku, E.G., Jackson, T.J., Lakshmi, V., Chan, T.K. & Nghiem, S.V. (2003). Soil moisture

971   retrieval from AMSR-E. *IEEE Transactions on Geoscience and Remote Sensing, 41*,

972   215-229

973 Oliva, R., Daganzo, E., Kerr, Y.H., Mecklenburg, S., Nieto, S., Richaume, P. & Gruhier, C.

974   (2012). SMOS Radio Frequency Interference Scenario: Status and Actions Taken to

975   Improve the RFI Environment in the 1400–1427-MHz Passive Band. *IEEE*

976   *Transactions on Geoscience and Remote Sensing, 50*, 1427-1439

977 Oliva, R., Daganzo, E., Richaume, P., Kerr, Y., Cabot, F., Soldo, Y., Anterrieu, E., Reul, N.,

978   Gutierrez, A., Barbosa, J. & Lopes, G. (2016). Status of Radio Frequency Interference

979   (RFI) in the 1400–1427 MHz passive band based on six years of SMOS mission.

980   *Remote Sensing of Environment, 180*, 64-75

981   Owe, M. & Van de Griend, A.A. (1998). Comparison of soil moisture penetration depths for

982   several bare soils at two microwave frequencies and implications for remote sensing.

983   *Water Resources Research, 34*, 2319-2327

984   Owe, M., de Jeu, R. & Walker, J. (2001). A methodology for surface soil moisture and

985   vegetation optical depth retrieval using the microwave polarization difference index.

986   *IEEE Transactions on Geoscience and Remote Sensing, 39*, 1643-1654

987   Parinussa, R.M., Holmes, T.R.H., Yilmaz, M.T. & Crow, W.T. (2011). The impact of land

988   surface temperature on soil moisture anomaly detection from passive microwave

989   observations. *Hydrology and Earth System Sciences, 15*, 3135-3151

990   Parrens, M., Zakharova, E., Lafont, S., Calvet, J.C., Kerr, Y., Wagner, W. & Wigneron, J.P.

991   (2012). Comparing soil moisture retrievals from SMOS and ASCAT over France.

992   *Hydrology and Earth System Sciences, 16*, 423-440

993   Parrens, M., Wigneron, J.-P., Richaume, P., Mialon, A., Al Bitar, A., Fernandez-Moran, R.,

994   Al-Yaari, A. & Kerr, Y.H. (2016). Global-scale surface roughness effects at L-band as

995   estimated from SMOS observations. *Remote Sensing of Environment, 181*, 122-136

996   Piepmeier, J., Mohammed, P., De Amici, G., Kim, E., Peng, J., Ruf, C., Hanna, M., Yueh, S.

997   & Entekhabi, D. (2016). Soil Moisture Active Passive (SMAP) Project Algorithm

998   Theoretical Basis Document SMAP L1B Radiometer Data Product: L1B_TB

999   Rautiainen, K., Lemmetyinen, J., Pulliainen, J., Vehvilainen, J., Drusch, M., Kontu, A.,

1000   Kainulainen, J. & Seppanen, J. (2012). L-Band Radiometer Observations of Soil

1001   Processes in Boreal and Subarctic Environments. *IEEE Transactions on Geoscience*

1002   *and Remote Sensing, 50*, 1483-1497

1003   Reichle, R., Draper, C., Koster, R., Liu, A., Girotto, M., Mahanama, S. & De Lannoy, G.

1004   (2016). Assessment of MERRA-2 land surface hydrology estimates. *Journal of*

1005   *Climatology, submitted*

1006   Reichle, R.H., Koster, R.D., De Lannoy, G.J.M., Forman, B.A., Liu, Q., Mahanama, S.P.P. &

1007   Touré, A. (2011). Assessment and Enhancement of MERRA Land Surface Hydrology

1008   Estimates. *Journal of Climate, 24*, 6322-6338

1009   Rondinelli, W.J., Hornbuckle, B.K., Patton, J.C., Cosh, M.H., Walker, V.A., Carr, B.D. &

1010   Logsdon, S.D. (2015). Different Rates of Soil Drying after Rainfall Are Observed by

1011   the SMOS Satellite and the South Fork in situ Soil Moisture Network. *Journal of*

1012   *Hydrometeorology, 16*, 889-903

1013   Saleh, K., Wigneron, J.-P., de Rosnay, P., Calvet, J.-C. & Kerr, Y. (2006). Semi-empirical

1014   regressions at L-band applied to surface soil moisture retrievals over grass. *Remote*

1015   *Sensing of Environment, 101*, 415-426

1016   Sanchez, N., Martinez-Fernandez, J., Scaini, A. & Perez-Gutierrez, C. (2012). Validation of

1017   the SMOS L2 Soil Moisture Data in the REMEDHUS Network (Spain). *Geoscience*

1018   *and Remote Sensing, IEEE Transactions on, 50*, 1602-1611

1019   Schaefer, G.L., Cosh, M.H. & Jackson, T.J. (2007). The USDA Natural Resources

1020   Conservation Service Soil Climate Analysis Network (SCAN). *Journal of*

1021   *Atmospheric and Oceanic Technology, 24*, 2073-2077

1022   Schmugge, T., T. Wilheit, W. Webster, Jr. & Gloersen, P. (1976). Remote sensing of soil

1023   moisture with microwave radiometers-II. *Nat. Aeronautics and Space Admin., NASA*

1024   *Tech. Note D-8321*

1025   Seneviratne, S.I., Corti, T., Davin, E.L., Hirschi, M., Jaeger, E.B., Lehner, I., Orlowsky, B. &

1026   Teuling, A.J. (2010). Investigating soil moisture–climate interactions in a changing

1027   climate: A review. *Earth-Science Reviews, 99*, 125-161

1028   Smith, A.B., Walker, J.P., Western, A.W., Young, R.I., Ellett, K.M., Pipunic, R.C., Grayson,

1029   R.B., Siriwardena, L., Chiew, F.H.S. & Richter, H. (2012). The Murrumbidgee soil

1030   moisture monitoring network data set. *Water Resources Research, 48*, W07701

1031   Tagesson, T., Fensholt, R., Guiro, I., Rasmussen, M.O., Huber, S., Mbow, C., Garcia, M.,

1032   Horion, S., Sandholt, I., Holm-Rasmussen, B., Göttsche, F.M., Ridler, M.-E., Olén,

1033   N., Lundegard Olsen, J., Ehammer, A., Madsen, M., Olesen, F.S. & Ardö, J. (2015).

1034   Ecosystem properties of semiarid savanna grassland in West Africa and its

1035   relationship with environmental variability. *Global Change Biology, 21*, 250-264

1036   Taylor, K.E. (2001). Summarizing multiple aspects of model performance in a single

1037   diagram. *Journal of Geophysical Research: Atmospheres, 106*, 7183-7192

1038   Ulaby, F.T., Dubois, P.C. & van Zyl, J. (1996). Radar mapping of surface soil moisture.

1039   *Journal of Hydrology, 184*, 57-84

1040   Van der Schalie, R., Kerr, Y.H., Wigneron, J.P., Rodríguez-Fernández, N.J., Al-Yaari, A. &

1041   Jeu, R.A.M.d. (2016). Global SMOS Soil Moisture Retrievals from The Land

1042   Parameter Retrieval Model. *International Journal of Applied Earth Observation and*

1043   *Geoinformation, 45, Part B*, 125-134

1044   Vittucci, C., Ferrazzoli, P., Kerr, Y., Richaume, P., Guerriero, L., Rahmoune, R. & Laurin,

1045   G.V. (2016). Smos retrieval over forests: Exploitation of optical depth and tests of soil

1046   moisture estimates. *Remote Sensing of Environment, 180*, 115-127

1047   Wagner, W., Dorigo, W., Richard de Jeu, Diego Fernandez, Jerome Benveniste, Eva Haas &

1048   Ertl, M. (2012). Fusion of Active and Passive Microwave Observations to Create an

1049   Essential Climate Variable Data Record on Soil Moisture. *XII Congress of the*

1050   *International Society for Photogrammetry and Remote Sensing-Melbourne, Australia*

1051   Wang, J.R. & Choudhury, B.J. (1981). Remote sensing of soil moisture content, over bare

1052   field at 1.4 GHz frequency. *Journal of Geophysical Research: Oceans, 86*, 5277-5282

1053   Wang, J.R., O'Neill, P.E., Jackson, T.J. & Engman, E.T. (1983). Multifrequency

1054   Measurements of the Effects of Soil Moisture, Soil Texture, And Surface Roughness.

1055   *IEEE Transactions on Geoscience and Remote Sensing, GE-21*, 44-51

1056 Western, A.W., Zhou, S.-L., Grayson, R.B., McMahon, T.A., Blöschl, G. & Wilson, D.J.

1057   (2004). Spatial correlation of soil moisture in small catchments and its relationship to

1058   dominant spatial hydrological processes. *Journal of Hydrology, 286*, 113-134

1059 Wigneron, J.-P., Chanzy, A., Calvet, J.-C. & Bruguier, N. (1995). A simple algorithm to

1060   retrieve soil moisture and vegetation biomass using passive microwave measurements

1061   over crop fields. *Remote Sensing of Environment, 51*, 331-341

1062 Wigneron, J.P., Calvet, J.C., Pellarin, T., Van de Griend, A.A., Berger, M. & Ferrazzoli, P.

1063   (2003). Retrieving near-surface soil moisture from microwave radiometric

1064   observations: current status and future plans. *Remote Sensing of Environment, 85*,

1065   489-506

1066 Wigneron, J.P., Calvet, J.C., De Rosnay, P., Kerr, Y., Waldteufel, P., Saleh, K., Escorihuela,

1067   M.J. & Kruszewski, A. (2004). Soil moisture retrievals from biangular L-band passive

1068   microwave observations. *Geoscience and Remote Sensing Letters, IEEE, 1*, 277-281

1069 Wigneron, J.P., Kerr, Y., Waldteufel, P., Saleh, K., Escorihuela, M.J., Richaume, P.,

1070   Ferrazzoli, P., de Rosnay, P., Gurney, R., Calvet, J.C., Grant, J.P., Guglielmetti, M.,

1071   Hornbuckle, B., Mätzler, C., Pellarin, T. & Schwank, M. (2007). L-band Microwave

1072   Emission of the Biosphere (L-MEB) Model: Description and calibration against

1073   experimental data sets over crop fields. *Remote Sensing of Environment, 107*, 639-655

1074 Wigneron, J.P., Chanzy, A., Kerr, Y.H., Lawrence, H., Shi, J., Escorihuela, M.J., Mironov,

1075   V., Mialon, A., Demontoux, F., Rosnay, P.d. & Saleh-Contell, K. (2011). Evaluating

1076   an Improved Parameterization of the Soil Emission in L-MEB. *IEEE Transactions on*

1077   *Geoscience and Remote Sensing, 49*, 1177-1189

1078 Zeng, J., Chen, K.S., Bi, H. & Chen, Q. (2016). A Preliminary Evaluation of the SMAP

1079   Radiometer Soil Moisture Product Over United States and Europe Using Ground-

1080   Based Measurements. *IEEE Transactions on Geoscience and Remote Sensing, PP*, 1-

1081   0

1082

1083

1084

1085

1086

1087

1088

1089

1090

1091

1092

1093

1094

1095

1096

1097

1098

"LIST OF FIGURE CAPTIONS"

1100

1101 **Fig. 10** IGBP (International Geosphere Biosphere Programme) land cover classification
1102 (Friedl et al., 2010) with the locations of the different *in situ* soil moisture sites (a) over
1103 Australia (b), the USA (c), and Africa and Europe (d).

1104 **Fig. 11** The LRM (local regression method) algorithm: inputs (in blue), calibration step (in
1105 red), and soil moisture production step (in green).

1106 **Fig. 12** Global inter-comparison between SMOS and SMAP TBs during the Apr 2015-Jul
1107 2016 at both polarizations vertical (V-pol; left) and horizontal (H-pol; right): (a & e)
1108 correlation, (b & f) RMSE, (c & g) Bias, and (d &h) UnbRMSE. Pixels with a number of
1109 observations lower than 15 are indicated as blank areas.

1110 **Fig. 13** Global inter-comparison between SMOS and SMAP soil moisture retrievals during
1111 the Apr 2015-Jul 2016: (a) correlation, (b) RMSE, (c) Bias, and (d) UnbRMSE. Pixels with a
1112 number of observations lower than 15 are indicated as blank areas.

1113 **Fig. 14** Regression coefficients of Eq. 1 calibrated using SMOS Level 3 TB and soil moisture
1114 in 2013-2014 (a): intercept (a_0), (b) slope of regression line corresponding to the horizontal
1115 polarization (a_1), and (c) slope of regression line corresponding to the vertical polarization
1116 (a_2).

1117 **Fig. 15** Comparison between the soil moisture values computed from the SMOS TB data
1118 using LRM (SMOS_Reg) and the SMOS official level 3 soil moisture product in 2013-2014:
1119 (a) correlation, R and (b) RMSE (m^3/m^3). Pixels with a number of observations lower than 15
1120 are indicated as blank areas.

1121 **Fig. 16** Comparison between the SMAP-derived soil moisture applying LRM (SMAP_Reg)
1122 using two different soil temperature products: GEOS-5 (left) and ECMWF (right) and the
1123 SMAP level 3 soil moisture product (SMAP_SCA) from Apr 2015 to Jul 2016: (top)
1124 correlation, R (-) and (bottom) RMSE (m^3/m^3).

1125 **Fig. 17** Taylor's diagrams for SMAP_Reg (in red), SMAP_SCA (in blue), and SMOSL3 (in
1126 green) over the FMI, DAHRA, iRON, and Oznet (upper panel), over SCAN, PBO-H2O,
1127 REMEDHUS, and RSMN sites (middle panel), and over SNOTEL, USCRN, and
1128 SMOSMANIA sites (lower panel).

1129 **Fig. 18** Bar charts showing Bias (m^3/m^3), R, RMSE (m^3/m^3), and UnbRMSE (m^3/m^3)
1130 between SMAP_SCA (in blue), SMAP_Reg (in red), and SMOSL3 (in green) and the
1131 observed soil moisture over the 11 networks used in this study.

1132 **"LIST OF TABLES CAPTIONS"**

1133 **Table 3** Regression coefficients of Eq. 1 calibrated using SMOS Level 3 TB and soil
1134 moisture in 2013-2014: a_0 represents the intercept, a_1 and a_2 represent the slope of regression
1135 line corresponding to H-pol and V- pol, respectively.

1136 **Table 4** Statistics of the evaluation of the SMAP_Reg, SMAP_SCA, and SMOSL3 against
1137 ground based measurements. The average (median for R instead of "average" as correlation is
1138 not additive) values were only computed for sites that have p_value < 0.05 and number of
1139 observations was higher than 15.

1140
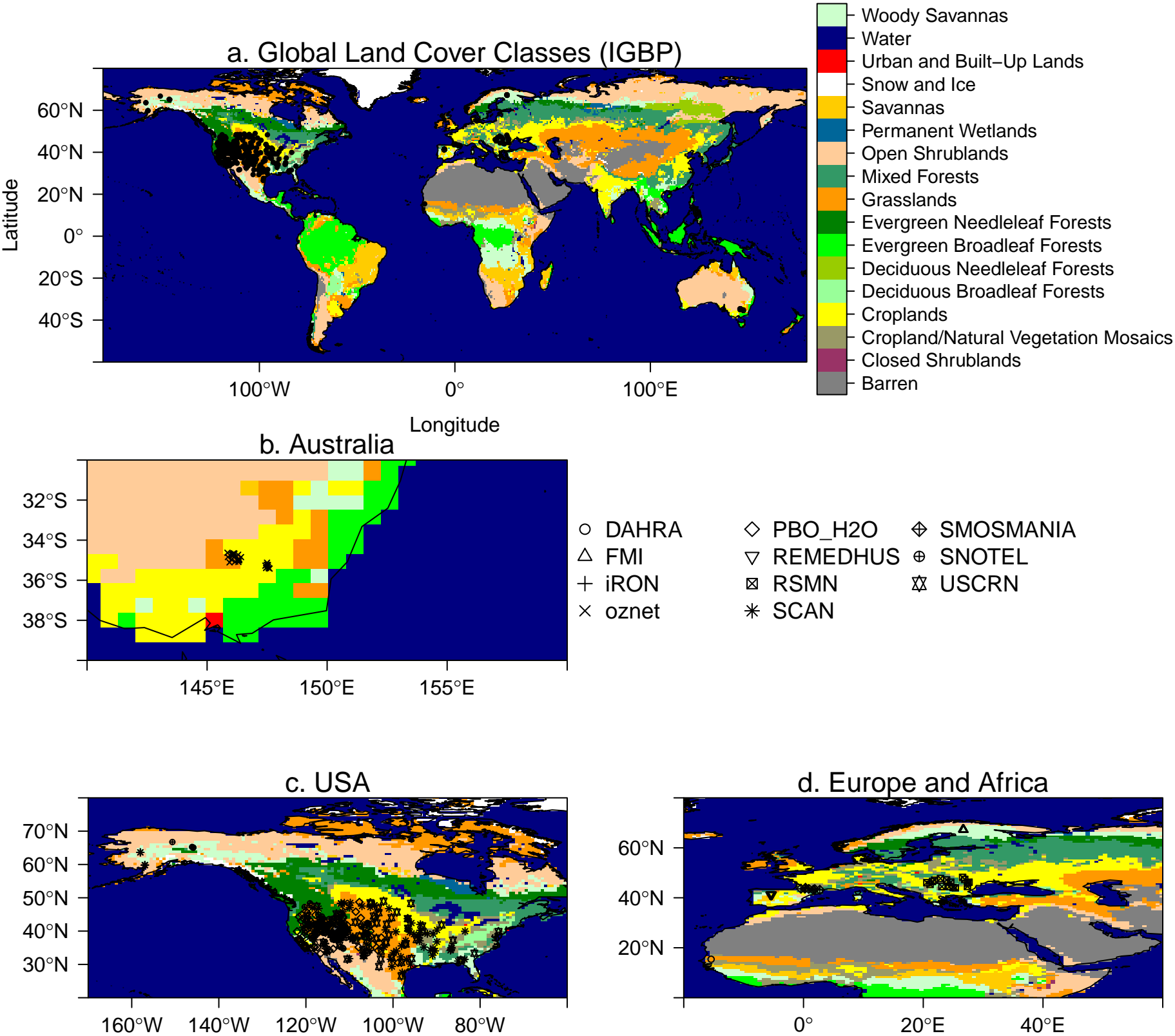
a. Global Land Cover Classes (IGBP)

Legend:
- Woody Savannas
- Water
- Urban and Built−Up Lands
- Snow and Ice
- Savannas
- Permanent Wetlands
- Open Shrublands
- Mixed Forests
- Grasslands
- Evergreen Needleleaf Forests
- Evergreen Broadleaf Forests
- Deciduous Needleleaf Forests
- Deciduous Broadleaf Forests
- Croplands
- Cropland/Natural Vegetation Mosaics
- Closed Shrublands
- Barren

b. Australia

- ○ DAHRA
- △ FMI
- + iRON
- × oznet
- ◇ PBO_H2O
- ▽ REMEDHUS
- ⊠ RSMN
- ✳ SCAN
- ⊕ SMOSMANIA
- ⊕ SNOTEL
- ⊠ USCRN

c. USA

d. Europe and Africa

Soil moisture (SM) (SMOSL3) (2013:2014)

Brightness temperature TB H&V (SMOSL3) Soil temperature (T_G) (MERRA-Land) (2013:2014)

$$\ln(SM) = a_2\ln(1-(TB_V/T_G)) + a_1\ln(1-(TB_H/T_G)) + a_0$$

Calibration coefficients a_0, a_1, a_2 (2013:2014)

Calibration step

TB H&V (SMAPL3); T_G (GEOS-5) (Apr 2015 to Jul 2016)

$$\ln(SM) = a_2\ln(1-(TB_H/T_G)) + a_1\ln(1-(TB_V/T_G)) + a_0$$

SMAP-Reg soil moisture retrievals (Apr 2015 to Jul 2016)

Production step

Figure 3

V−Pol a : Correlation

H−Pol e : Correlation

b : RMSE (K)

f : RMSE (K)

c : Bias (K)

g : Bias (K)

d : UnbRMSE (K)

h : UnbRMSE (K)

a : Correlation

c : Bias (m^3/m^3)

b : RMSE (m^3/m^3)

d : UnbRMSE (m^3/m^3)

(a) Intercept

(b) H−Pol

(c) V−Pol
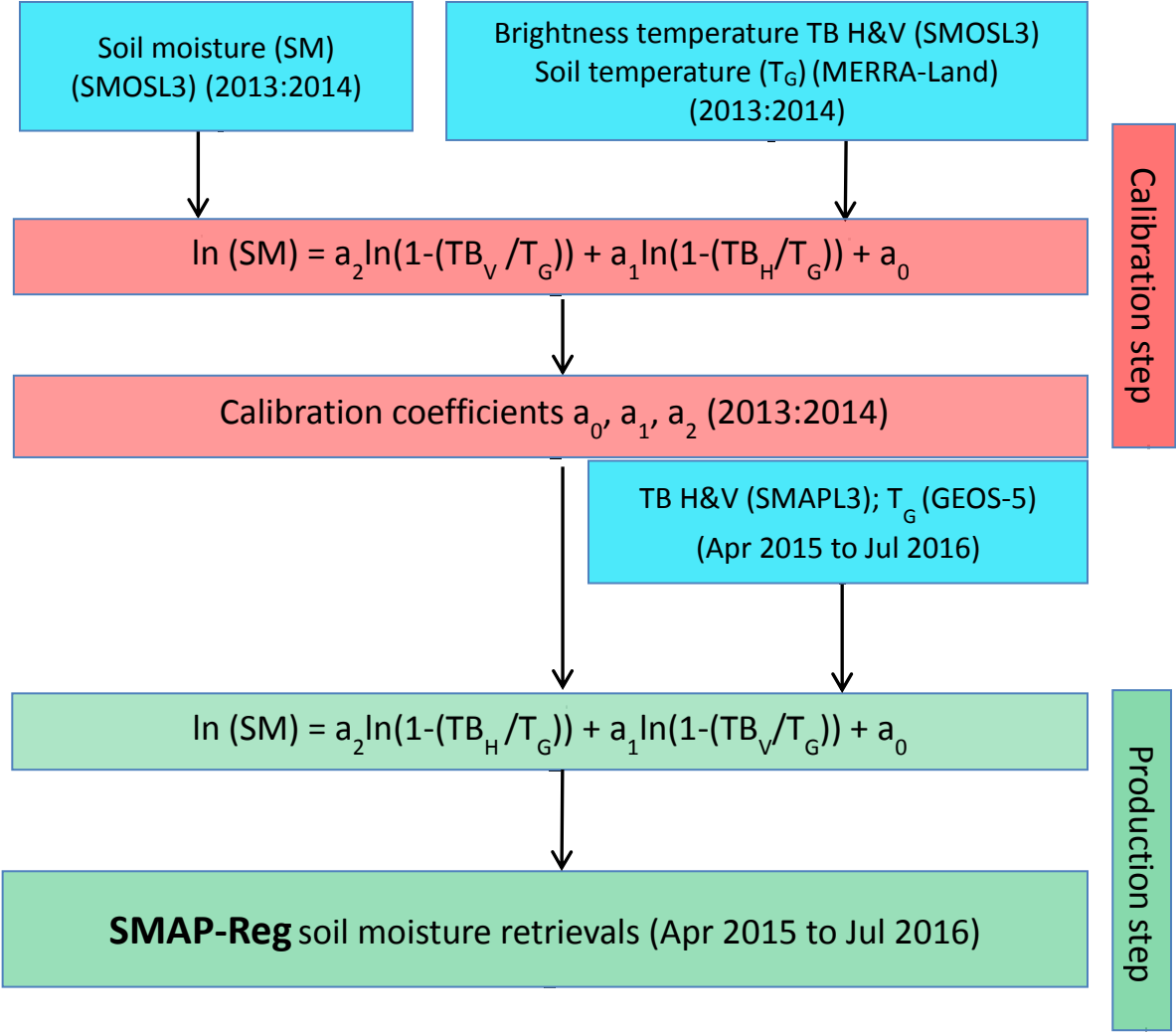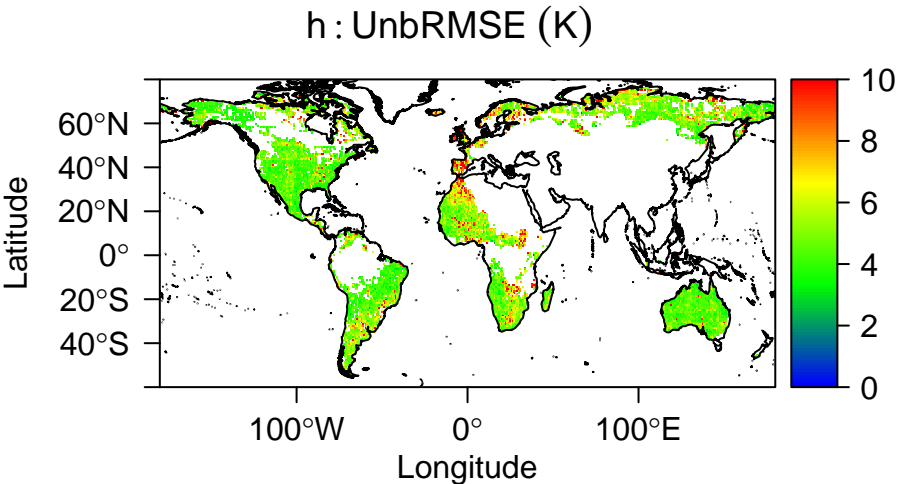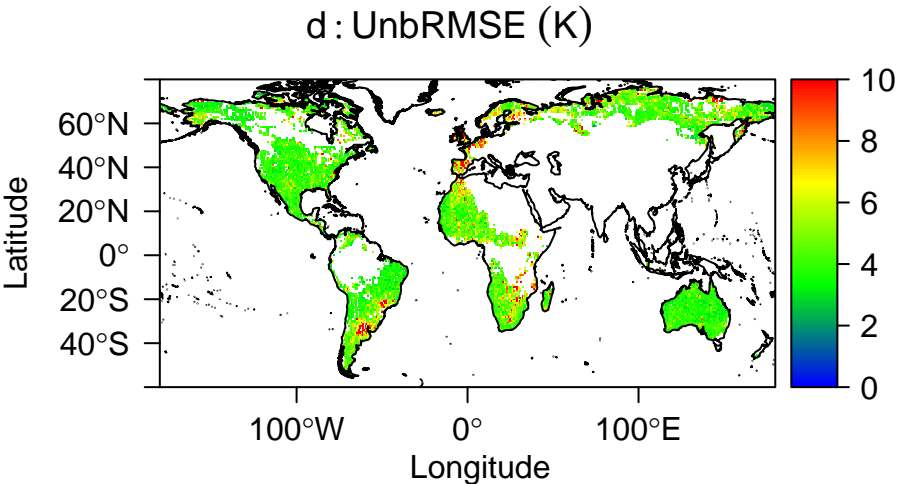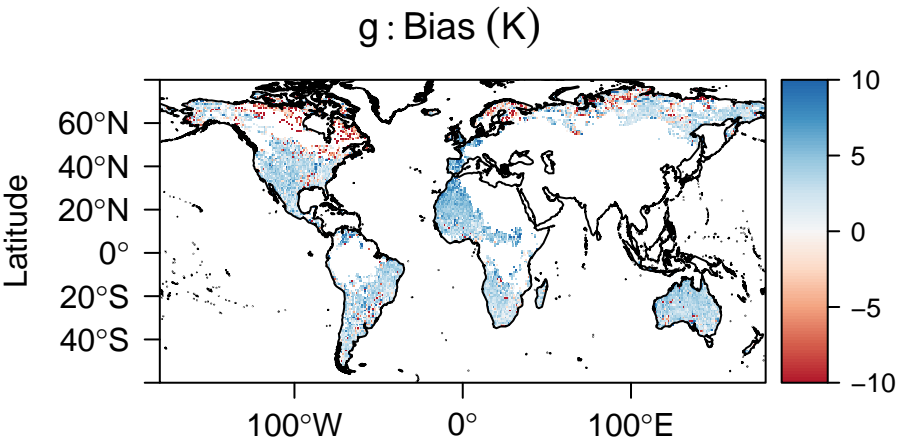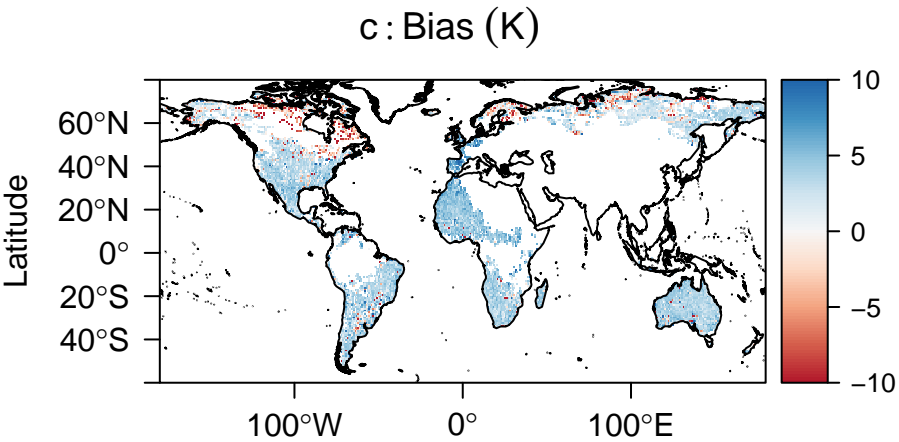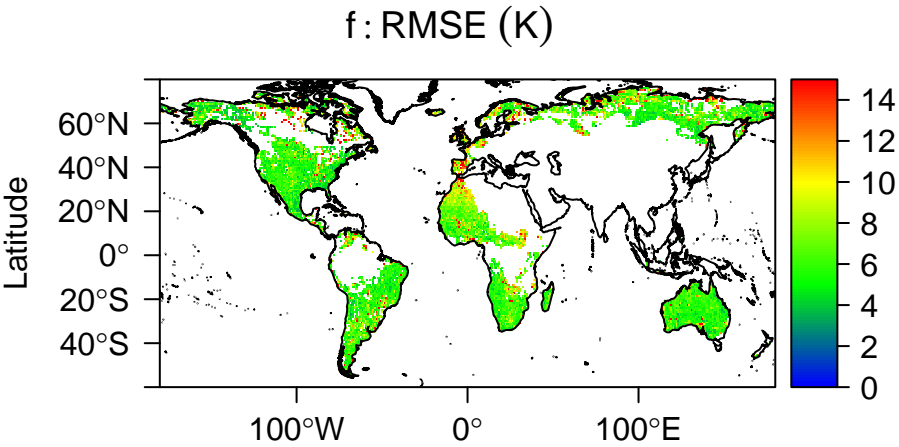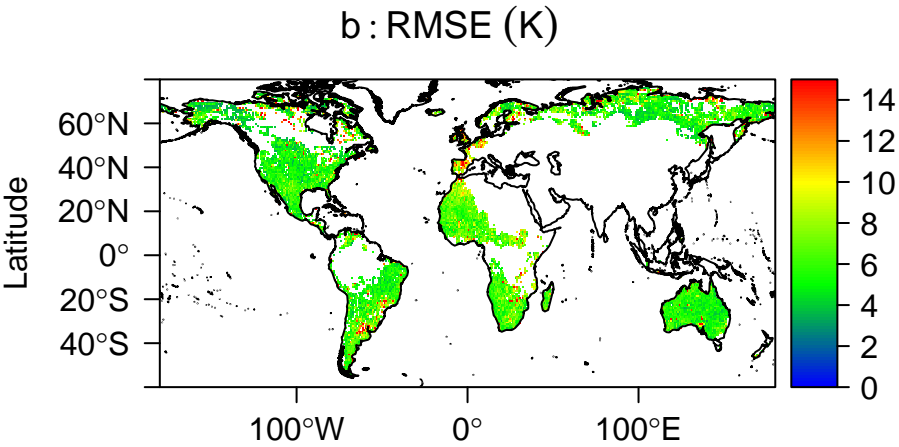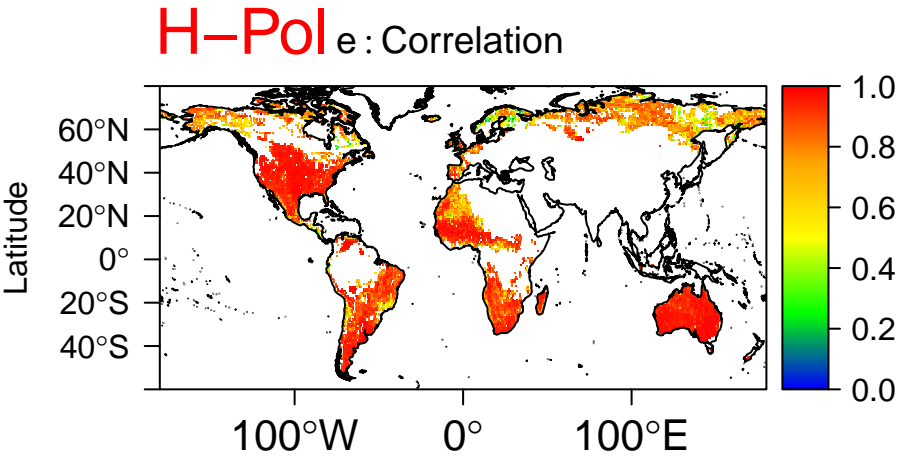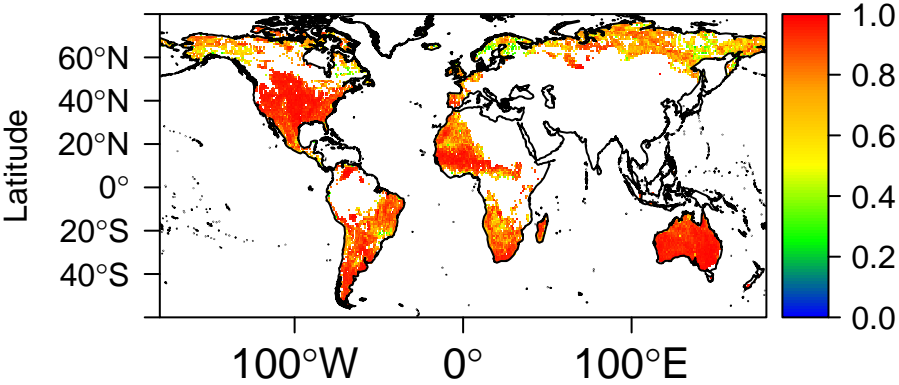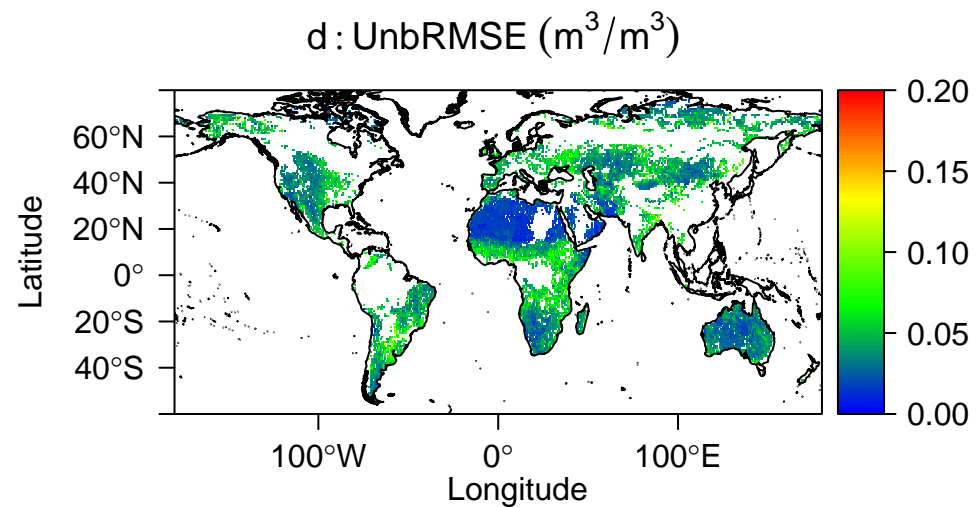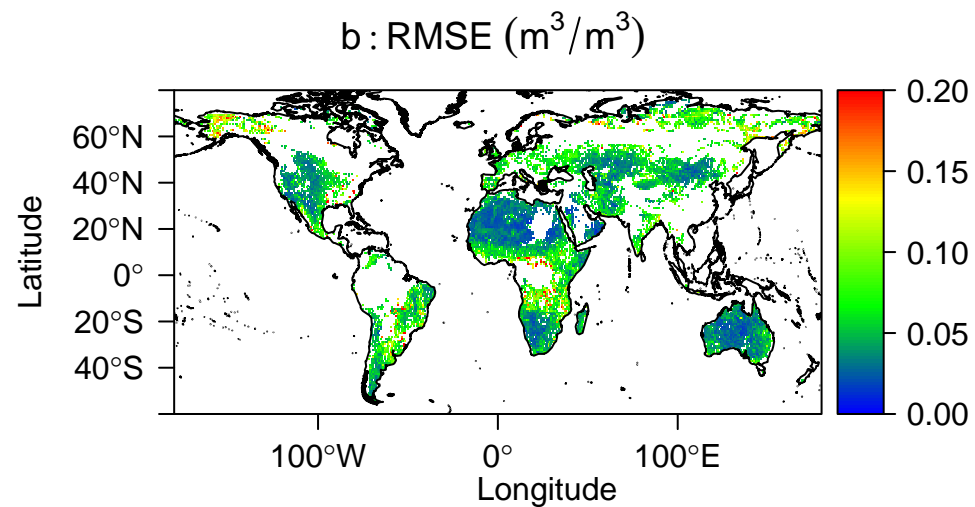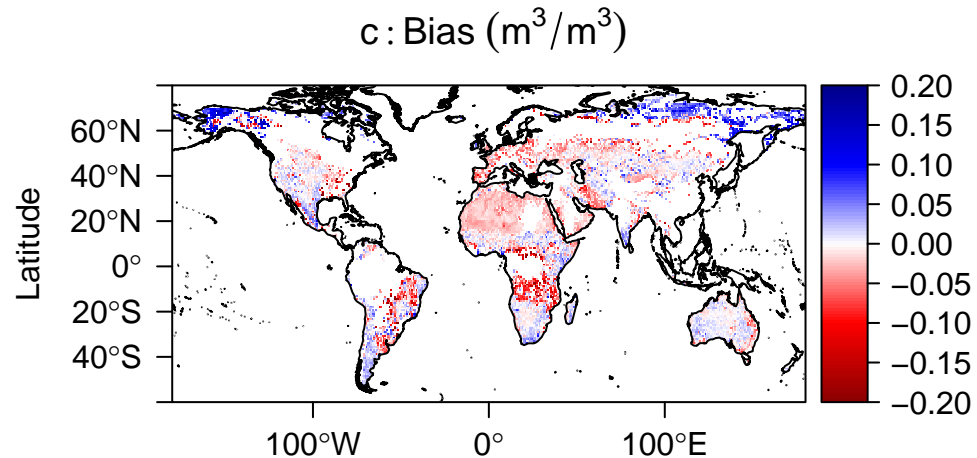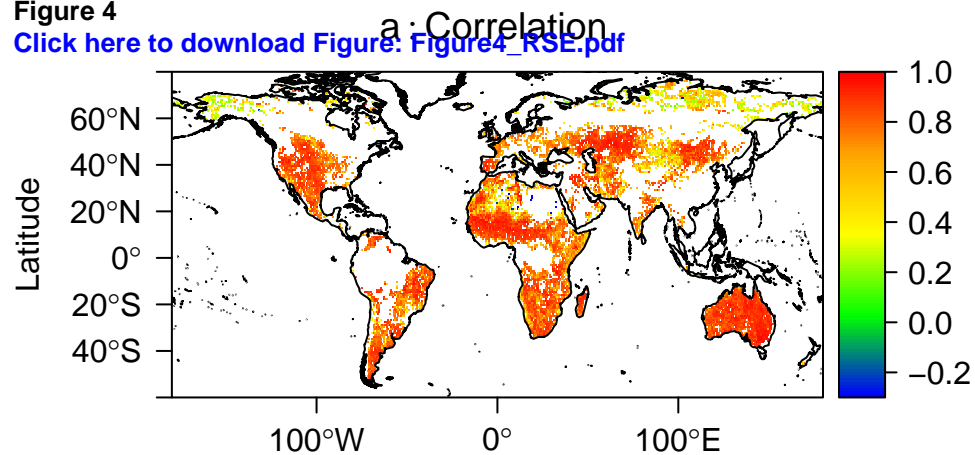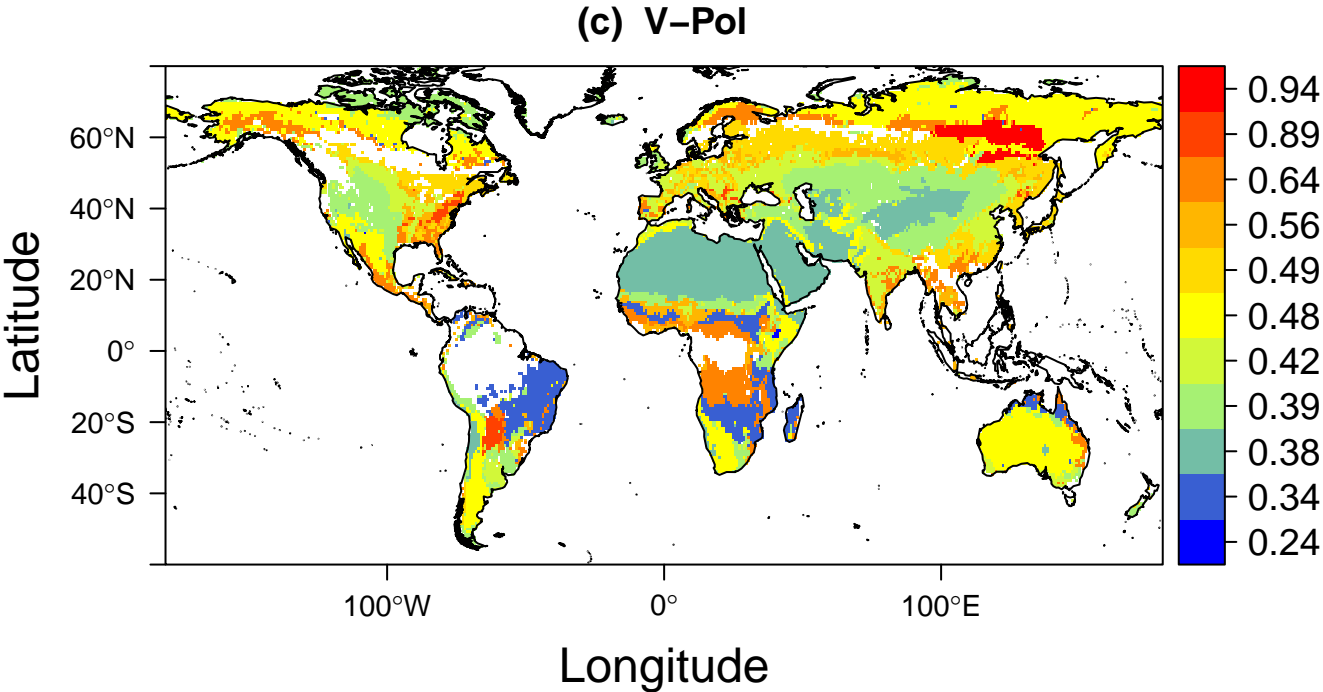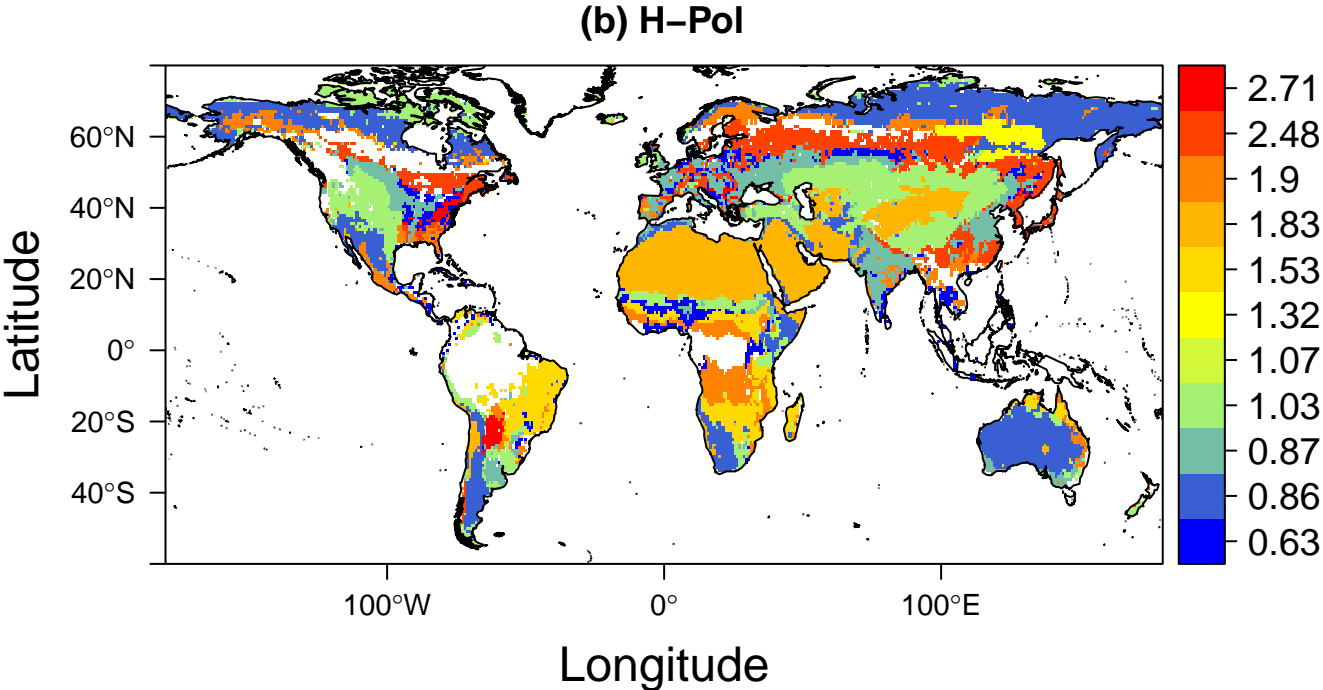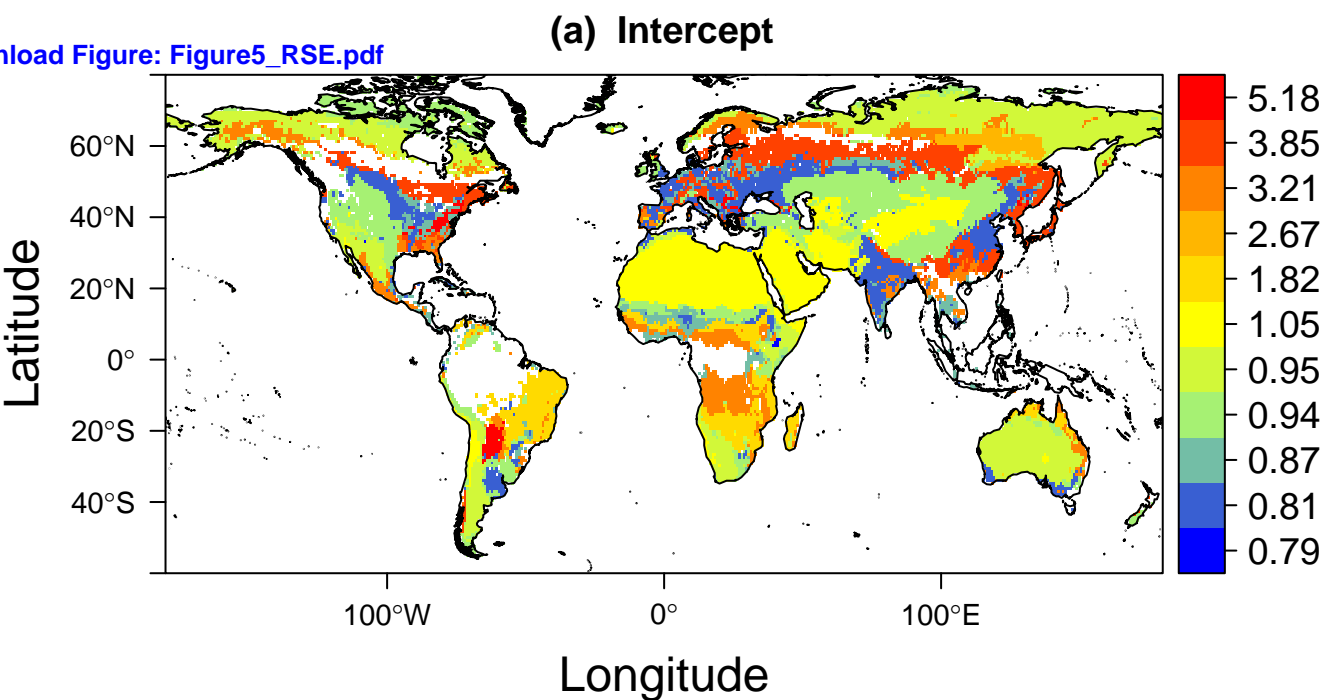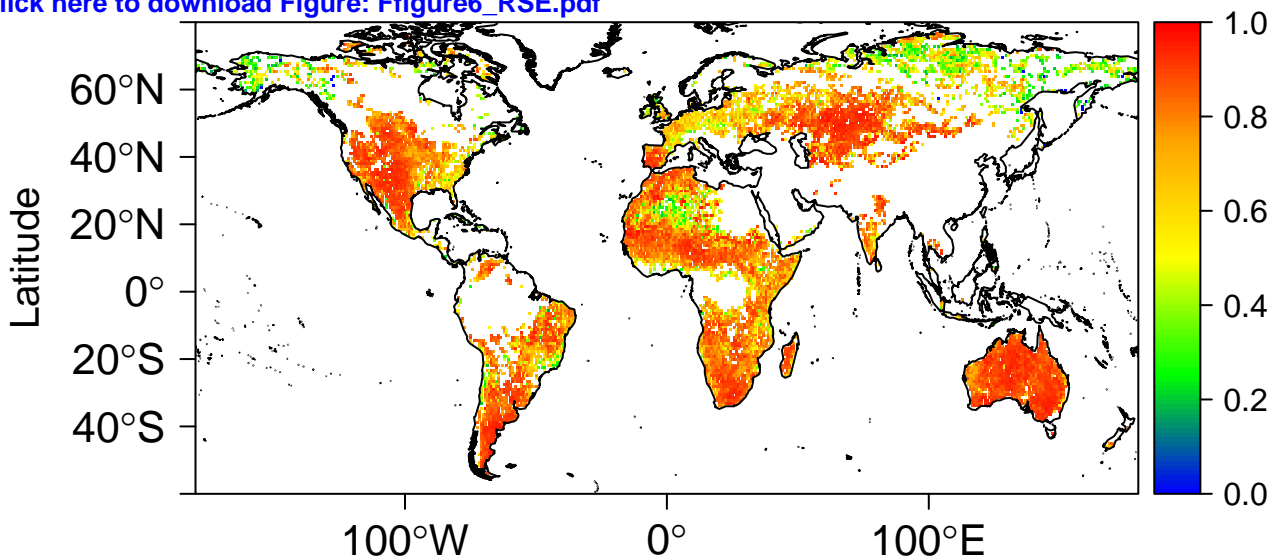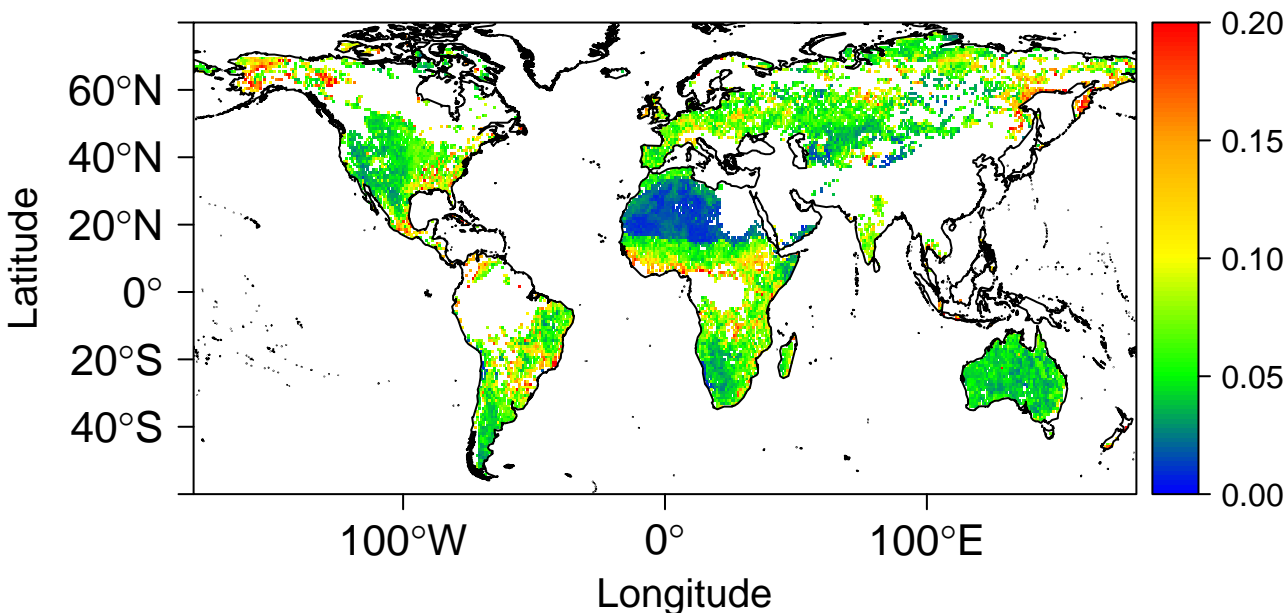
Figure 6

(a) Correlation

(b) RMSE

Figure 7

a: Correlation (GEOS−5)
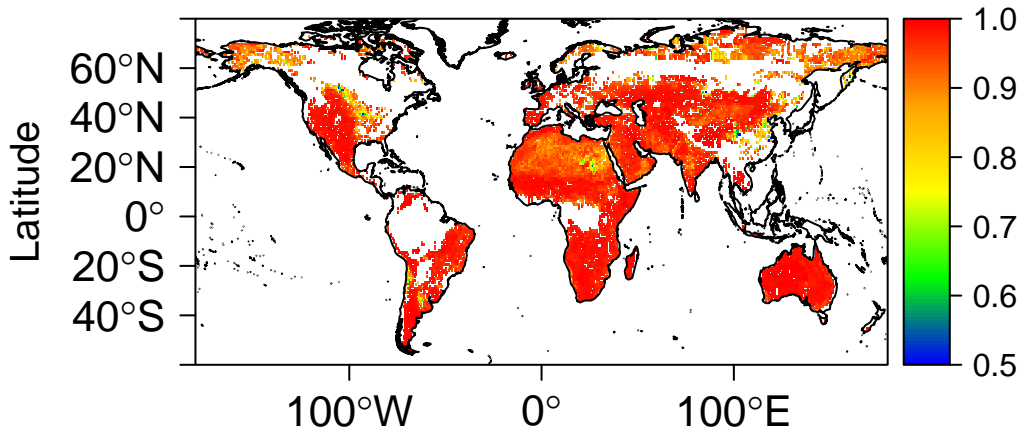
c: Correlation (ECMWF)
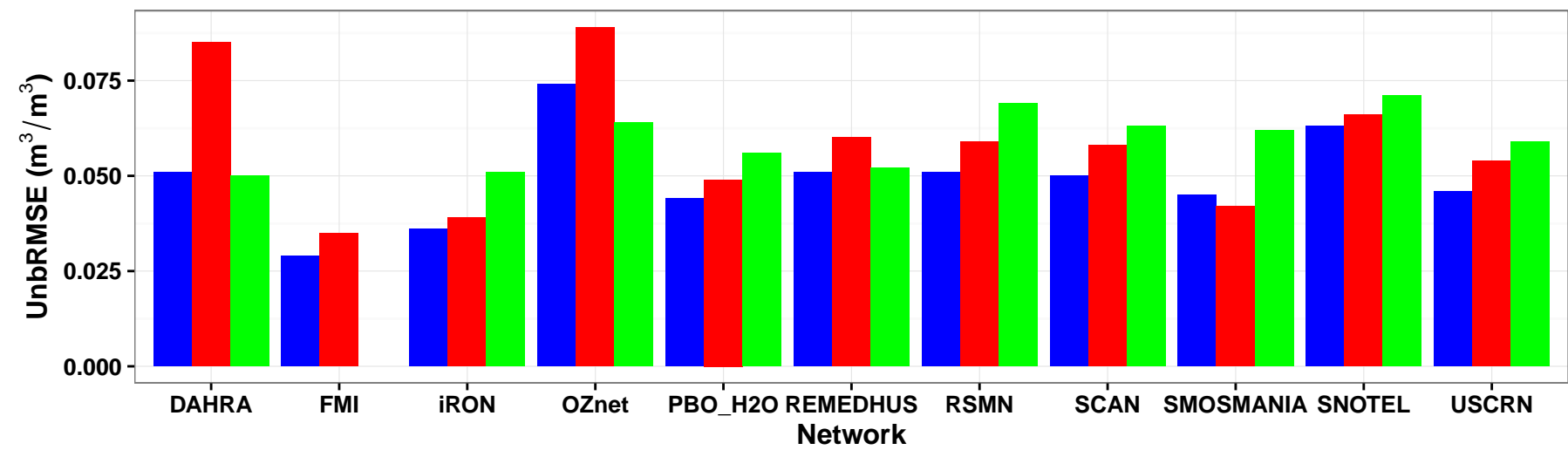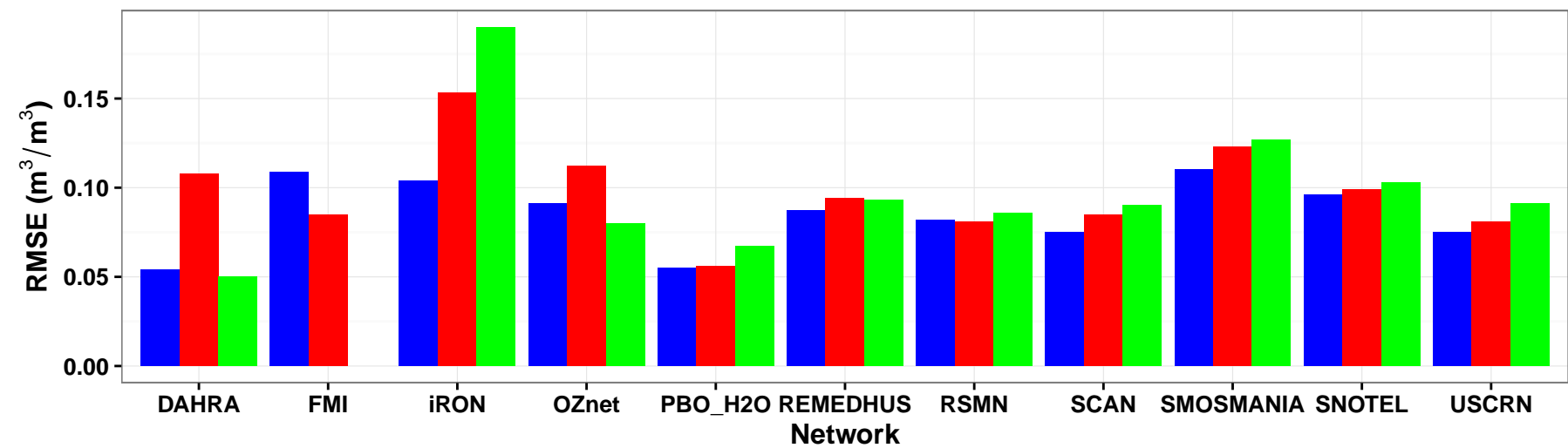
b: RMSE (GEOS−5)

d: RMSE (ECMWF)